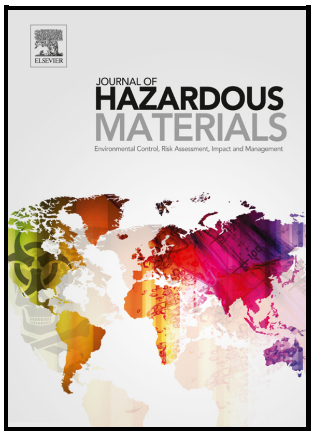

Evidence of hexavalent chromium formation and changes of Cr speciation after laboratory-simulated fires of composted tannery sludges long-term amended agricultural soils

Ida Rascio, Ignazio Allegretta, Concetta Eliana Gattullo, Carlo Porfido, Gian Paolo Suranna, Roberto Grisorio, Kathryn M. Spiers, Gerald Falkenberg, Roberto Terzano

PII: S0304-3894(22)00907-4

DOI: https://doi.org/10.1016/j.jhazmat.2022.129117

Reference: HAZMAT129117

To appear in: *Journal of Hazardous Materials*

Received date: 25 February 2022
Revised date: 12 April 2022
Accepted date: 6 May 2022

Please cite this article as: Ida Rascio, Ignazio Allegretta, Concetta Eliana Gattullo, Carlo Porfido, Gian Paolo Suranna, Roberto Grisorio, Kathryn M. Spiers, Gerald Falkenberg and Roberto Terzano, Evidence of hexavalent chromium formation and changes of Cr speciation after laboratory-simulated fires of composted tannery sludges long-term amended agricultural soils, *Journal of Hazardous Materials,* (2022) doi:https://doi.org/10.1016/j.jhazmat.2022.129117

Evidence of hexavalent chromium formation and changes of Cr speciation after laboratory-simulated fires of composted tannery sludges long-term amended agricultural soils

Ida Rascio[a], Ignazio Allegretta[a], Concetta Eliana Gattullo[a], Carlo Porfido[a], Gian Paolo Suranna[b,c], Roberto Grisorio[b,c], Kathryn M. Spiers[d], Gerald Falkenberg[d], Roberto Terzano[a,*]

[a] Department of Soil, Plant and Food Sciences, University of Bari "Aldo Moro", Via G. Amendola 165/A, 70126 Bari, Italy

[b] Dipartimento di Ingegneria Civile, Ambientale, del Territorio, Edile e di Chimica (DICATECh), Politecnico di Bari, Via Orabona 4, 70125 Bari, Italy

[c] CNR NANOTEC – Istituto di Nanotecnologia, Via Monteroni, 73100 Lecce, Italy

[d] Deutsches Elektronen-Synchrotron DESY, Notkestr. 85, 22607 Hamburg, Germany

*Corresponding author: Roberto Terzano, Department of Soil, Plant and Food Sciences, University of Bari "Aldo Moro", Via G. Amendola 165/A, 70126 Bari, Italy – e-mail: roberto.terzano@uniba.it – Tel. +39 080 5442852 – Fax: +39 080 5442850

Abstract

Controlled or accidental fires can impact agricultural soils amended with composted organic materials since high temperatures cause fast organic matter (OM) mineralization and soil properties modifications. During these events, potentially toxic elements (PTEs) associated with OM can be released and change their distribution and speciation thus becoming a threat to the environment and to crops.

In this study, we investigated the changes of distribution and speciation of chromium in soils long-term amended with compost obtained from tannery sludges, after simulating fires of different intensity (300, 400 and 500°C) likely to occur on agricultural soils. A combination of conventional soil chemical analyses and bulk and (sub)micro X-ray analyses allowed the observation of the

formation of hexavalent chromium and changes of chromium speciation. Specifically, a strong decrease of Cr-OM associations was found with increasing temperature in favour of Cr-iron (hydr)oxides interactions and $CaCrO_4$ formation. These data provide first evidence that fires can transform OM-stabilized Cr into more mobile, available and toxic Cr-forms potentially accessible for plant uptake, thus posing a risk for the food chain and the environment.

Keywords: organic matter mineralization, potentially toxic elements, X-ray analyses, synchrotron

Environmental Implication

In many parts around the globe, tannery waste has been applied to agricultural soils to improve organic matter (OM) content and provide micronutrients for plant nutrition. The high amounts of Cr present in these materials are complexed and stabilized by the OM which also prevents Cr(III) from oxidation to more toxic Cr(VI). However, these materials should be considered hazardous for soils and the environment. Indeed, in this paper we demonstrate that high temperatures, like those that can be reached during a fire on agricultural soils, can change Cr speciation making it potentially more available and more toxic.

1. Introduction

Soil pollution is one of the main threats affecting soil health worldwide (Naidu et al., 2021). In particular, pollution of agricultural soils arouses great concern due to risks of transferring contaminants from soil to plants and, through the food chain, to livestock and humans (Kabata-Pendias and Mukherjee, 2007). The use of organic and inorganic fertilizers and improvers (e.g., obtained from agro-industrial by-products, sewage sludge and wastewaters) represents one of the main causes of agricultural soils contamination (Donner et al., 2011; Shukla et al., 2017). These practices have increased in reason of the growing need of recycling by-products, especially treated biomasses (Sánchez-Monedero et al., 2004). If not properly treated and/or controlled, these materials may become a source of pollution by introducing in the environment huge amounts of contaminants that can accumulate in soils over the years (McGrath et al., 2001). Among the biosolids used in agriculture, sewage sludge and composted organic wastes are the most employed all around the world as they can improve soil health through organic carbon enrichment and slow release of macro and micronutrients for plant growth (Kumar et al., 2017; Naidu et al., 2021). However, together with the supply of beneficial elements and the positive effects on soil properties, also potentially dangerous elements can be introduced by these practices, as in the case of chromium-containing fertilizers obtained from tannery sludges (Ciavatta et al., 2012).

It is known that a large Cr-contamination of soils all around the world has arisen from the common practice of land-based disposal of tannery wastes. In these wastes, the dominant Cr species is usually the thermodynamically stable, non-toxic and immobile form, Cr(III) (López-Luna et al., 2009).

As tannery sludge contains high concentrations of Cr, its direct application to soil may cause environmental contamination. However, it can be reused for agricultural purposes as soil amendment or organic fertilizer after composting (Silva et al., 2014).

In general, Cr behaviour in soil depends on several factors: pH and redox potential, Cr oxidation state, amount of organic matter and of certain reactive minerals (e.g., Fe and Mn oxides), presence of electron donors or acceptors, competing ions and complexing agents (Adriano, 2001). Chromium is immobile under most soil conditions because of adsorption on soil colloids and the formation of insoluble complexes with hydroxides and organic ligands (Shi et al., 2020).

In a previous study, Gattullo et al. (2020) observed that the presence of high concentrations of OM (about 20%) favoured the immobilization and stabilization of Cr in two agricultural soils amended

for more than 10 years with compost derived from tannery sludges. In fact, this study revealed that Cr was mainly distributed in the most recalcitrant soil fractions, especially associated to OM, and that the risk of Cr(III) oxidation to Cr(VI) could be considered negligible as long as the OM content remained high (Gattullo et al., 2020). Indeed, Brunetti et al. (2012), studying durum wheat and barley growth on the same soils, did not observe any dangerous Cr uptake in these cereal crops, thus confirming the lack of risks associated to this polluted site.

However, OM mineralization by natural degradation processes or caused by more rapid and intense events like fires could change Cr distribution and speciation thus making it more mobile and/or more toxic. Indeed, fires can change soil properties and composition (including pH, redox potential, OM content, type of soil minerals) to such an extent that the distribution and speciation of potentially toxic elements (PTEs) can be affected (Terzano et al., 2021).

Hexavalent Cr formation in soils, via oxidation of Cr(III), is a topic of high environmental relevance due to Cr(VI) toxicity and carcinogenicity (USEPA, 1998). Generally, one of the main reported natural pathways for Cr(VI) formation in soils is the oxidation of Cr(III) at the surface of Mn(III/IV) oxides (Yu-Ling et al., 2006; Panichev et al., 2008, Shi et al. 2020). However, Cr(III) oxidation by O_2 is also thermodynamically feasible under certain conditions, but is generally of little importance as it is extremely slow at ambient temperature (Burton et al., 2019a). At higher temperatures, these kinetic limitations are overcome and the Cr(III) oxidation has been shown to readily occur (Burton et al., 2019b; Verbinnen et al., 2013; Wolf et al., 2008). In fact, as reported by Panichev et al. (2008), Cr(VI) can be formed during seasonable grass fires by Cr(III) oxidation at high temperature with atmospheric oxygen. Moreover, the oxidation of Cr(III) is also thermodynamically favoured in alkaline media in presence of $CaCO_3$, Na_2CO_3 or K_2CO_3, which are the major components of vegetation ash formed at 600–900°C (Panichev et al., 2008).

Nonetheless, scant information on Cr(III) oxidation due to high temperatures (such as those occurring during fire events) on agricultural soils is available. Indeed, fire events frequently occur in agricultural areas as an indirect effect of the rising aridity and global warming or caused by intentional burnings. In particular, controlled burning is still largely used by farmers as an agricultural practice in many parts of the world (Kumar et al., 2015). Generally, the temperatures and duration of fires on agricultural soils are not as high and persisting as in forest wildfires but, anyway, they can significantly impact soil properties (Terzano et al., 2021). Indeed, high soil temperatures may kill microbes and damage plant roots, degrade soil OM and affect soil nutrients content as well as water holding capacity; they can also enhance water repellence and the release of

ashes after the combustion of biomasses (Certini, 2005; Zavala et al., 2014). Fires can alter soil minerals, including highly reactive iron oxyhydroxides (Cudennec and Lecerf, 2005; Johnston et al., 2019). Soil properties can experience short-term, long-term, or permanent fire-induced changes, depending on severity and frequency of fires, as well as on post-fire climatic conditions (Certini, 2005).

The present work aims at studying Cr behaviour in highly polluted agricultural soils after fire simulations at laboratory-scale by using an integrated approach based on conventional analyses and X-ray based techniques, including synchrotron X-ray absorption spectroscopy (XAS) and X-ray absorption spectroscopy mapping at the microscale (μ-XANES). This kind of approach (from bulk down to (sub)micro scale) provided new and useful information about Cr speciation and distribution in heated soils and will help to predict possible environmental risks related to Cr-transformations in fire-affected soils.

2. Materials and methods

2.1. Site description and soil sampling

The investigated site is located in the South of Italy near the town of Altamura (Bari), in an agricultural area cultivated with durum wheat (*Triticum durum* Desf.). The extension of the contaminated area is of about 500 ha, as reported by Brunetti et al. (2012) and references therein. Soil sampling was performed at the beginning of July, about 3 weeks after wheat harvest, following the procedure described by Gattullo et al. (2020). Samples were collected from two different areas (A1 and A2) representing an extension of about 1 ha, together with a control sample taken from a nearby site.

The investigated site has been amended for more than 10 years with compost derived from tannery sludges, while the control soil has never been amended (Gattullo et al., 2020). As reported by Gattullo et al. (2020), A1 and A2 soils contained much higher concentrations of organic matter (OM) and potentially toxic elements (PTEs) than the control. In particular, Cr was the most abundant PTE (up to 5160 g kg^{-1}), and it was present only as Cr(III), as its oxidation to Cr(VI) was prevented by the high OM content.

2.2 Thermogravimetric analysis and laboratory-simulated fires

Soil samples (A1, A2 and control) were investigated by means of thermogravimetric analyses (TGA) to get information about the thermal behaviour of the soil samples, including transformations of organic and inorganic soil constituents (Terzano et al., 2021).

Preliminary information deriving from thermal analyses is usually adopted to set up thermal simulations on larger soil samples, as reported by Marcos et al. (2007) and Zhang et al. (2018).

A small amount (about 300 mg) of A1, A2 and control soil samples was loaded in a thermobalance (TGA/DSC Q600 TA Instruments) and heated from 30°C up to 900°C with a heating rate of 10°C min^{-1}, operating in static air condition mode. The obtained results were used to select the temperatures of the subsequent muffle furnace laboratory-heating experiments, as described below.

Three heat treatments were applied to 200 g aliquots of each soil sample (A1, A2 and control). Each aliquot was placed in a 20 cm diameter ceramic crucible, creating a soil layer of about 0.7 cm thickness, and heated in a muffle furnace (LT 9/14/B180, Nabertherm GmbH, Lilienthal, Germany) for 30 min up to 300°C, 400°C or 500°C. The heating time was selected according to studies on agricultural soils where such temperatures were recorded for about 30 min after burning crop residues on soil (Li et al., 2012).

After each thermal treatment, soil samples were allowed to cool to room temperature and then re-weighed to evaluate the resulting weight loss. Three replicates for each sample and for each thermal treatment were prepared. As evidenced in the insight carried out by Pereira et al. (2019), the muffle furnace is widely employed in laboratory-scale fire-simulation approaches as it allows the control of different variables and enables good experimental reproducibility.

2.3 Soil characterization at the bulk-scale

Soils were characterized for pH, electrical conductivity (EC), organic C content, total N content, total and active $CaCO_3$, available P, cation exchange capacity (CEC) and exchangeable bases, following the standard methodologies of soil analysis (Sparks, 1996).

Additionally, a representative aliquot of each soil sample was pulverized with an agate mortar and pestle and analysed for both the elemental and mineralogical composition by X-ray based techniques.

Total Cr content was measured by ED-XRF (NITON XL3t GOLDD with laboratory stand, Thermo Scientific Inc., Waltham, MA, USA). Samples were prepared and analysed following the procedure reported by Gattullo et al. (2020). Analytical accuracy of XRF measurements was evaluated analysing the standard reference materials BCR-CRM038 (coal fly ash) and CCRMP TILL-4 (soil).

For non-treated soils (N.T.), measurements were carried out on three different aliquots of one composite sample (about 20 kg) obtained by mixing three bulk samples collected from an area of about 4 m^2 for each soil considered (A1, A2 and Control), as described in Gattullo et al. (2020).

For thermally treated soils (300, 400 and 500), measurements were carried out on three different aliquots of the same composite sample described in the previous lines thermally treated in a muffle furnace separately for each temperature as reported in Section 2.2.

Soil mineralogical composition before and after heating treatments was obtained by X-ray powder diffraction (XRPD), using a Miniflex II X-ray diffractometer (Rigaku Corporation, Tokyo, Japan) equipped with a Cu-Kα X-ray source (30 kV, 15 mA, 450 W). Data were acquired between 3 and 70 2θ°, with a step width of 0.02° and a counting time of 2 s per step in continuous mode. Additional investigations on minor soil mineral constituents were performed by means of high resolution diffractometry using a θ/2θ PANalytical X'Pert pro MPD diffractometer equipped with a Cu Kα X-ray source (40kV, 40mA, 1600 W). Data were acquired between 5 and 85 2θ° with a step width of 0.02°.

Chromium plant-available fraction was assessed by extracting each soil sample with diethylenetriaminepentaacetic acid (DTPA) solution (0.005 mol l^{-1} DTPA, 0.01 mol l^{-1} $CaCl_2$, 0.1 mol l^{-1} triethanolamine, pH = 7.3) (Lindsay and Norvell, 1978) and analysing the extracts by ICP-OES (Thermo iCAP 6000 series, Thermo Fisher Scientific Inc., Waltham, MA, USA).

Chromium fractionation before and after thermal treatments was assessed by means of sequential chemical extractions, using a modified BCR sequential extraction procedure (SEP) (Sahuquillo et al. 1999), as described by Gattullo et al. (2020).

Total Cr(VI) concentration was determined after the alkaline digestion of soil samples (USEPA method 3060A, 1996), while the exchangeable Cr(VI) was extracted by shaking the soils for 30 min with a 5 mM K_2HPO_4/KH_2PO_4 buffer solution (pH 7.2) at a ratio of 1:4 (soil:buffer solution, w/v) (Bartlett and James, 1996). The Cr(VI) quantification in both extracts (total Cr(VI) and exchangeable Cr(VI)) was performed by the colorimetric assay with diphenylcarbazide (USEPA

Method 7196A, 1992). The detection limit of the assay is 0.0052 mg l^{-1}(Bartlett and James, 1996), corresponding to about 0.2 µg Cr(VI) g^{-1} of dry soil for the total Cr(VI), and 0.02 µg Cr(VI) g^{-1} of dry soil for the exchangeable Cr(VI) (Bartlett and James, 1996).

2.4 Soil characterization at the micro-scale

Soil thin sections (30-µm thickness) were prepared after embedding the soils in epoxy resin (L.R. White Resin, Polyscience Europe GmbH, Germany) (Allegretta et al., 2018), and were analysed with a micro X-ray fluorescence spectrometer (µXRF, M4 Tornado, Bruker Nano GmbH, Germany). Elemental distribution maps were acquired under vacuum (20 mbar) using a Rh tube X-ray source (50 kV, 600 µA, 30 W) with polycapillary optics and two 30 mm^2 XFlash® silicon drift detectors. X-ray maps were collected in stepping mode with an X-ray beam spot size of 25 µm (FWHM), a step size of 25 µm and an acquisition time of 100 ms per pixel. X-ray fluorescence hyperspectral data were subsequently processed using Bruker M4 software and a combination of PyMca 5.1.3 (Solé et al. 2007), Datamuncher (Alfeld and Janssens, 2015) and CTAnalyser (version 1.15.4.0 +, ©Bruker µ-CT) software in order to assess variations in both distribution and correlation of elements as well as changes of soil aggregate characteristics and size with the heating treatments.

2.5 Chromium distribution and speciation: synchrotron X-ray based analyses

Synchrotron X-ray based XAS and XRF analyses were performed both at the bulk- and micro-scale to study the speciation and distribution of Cr in the soils before and after the heating treatments. The analyses were performed at the PETRA III facility (DESY, Hamburg, Germany).

2.5.1 Bulk XAS analyses

Bulk XAS analyses were carried out at the mini-undulator beamline P65 (Applied X-ray Absorption Spectroscopy Beamline) at the Cr K-edge (5989 eV) (Welter et al., 2019). Incoming photon energy was modulated with a Si(111) double crystal monochromator, with an energy resolution of ~ 0.6 eV at the Cr K-edge. P65 provides an unfocused undulator beam (flux higher than 10^{11} ph s^{-1} in 0.5 x 1 mm^2) which is ideally suited for in situ investigations for all kinds of samples with sizes larger than

1 mm^2. Higher harmonics were efficiently suppressed by a pair of Si-plane mirrors. Fast energy scans are facilitated by continuous and simultaneous scanning of monochromator and undulator energy.

Spectra of reference compounds and samples were acquired simultaneously in transmission and fluorescence mode using respectively ions chambers with a path length of 5 cm and a Passivated Implanted Planar Silicon (PIPS) fluorescence detector. The samples or the references were oriented 45 degrees to the beam direction and PIPS diode. Ion chambers were filled with a gas mixture of N_2, Ar and Kr to approximately obtain 15%, 50% and 100% absorption for I0, I1 and I2 respectively. Samples and reference compounds were analysed at liquid He temperature of 20 K and 10^{-5} bar to avoid changes in Cr speciation due to intense X-ray irradiation.

2.5.1.1 Soils and reference compounds preparation

Soils (A1, A2 and control, both before and after heating treatments) were prepared by pulverizing each soil sample (about 200 mg) with an agate mortar and pestle and adding few drops (about 800µl) of Elvacite® 2046 (Malvern PanAnalytical, Malvern, United Kingdom) 15% w/w acetone solution as binding agent. Elvacite® solution was preliminary verified to not contain Cr. After acetone evaporation, powdered samples were pressed as tabs of 20 mm diameter and 0.7 mm thickness using a uniaxial press operating under vacuum at 10 tons cm^{-2}.

Similarly, a number of Cr-reference compounds were prepared as pellets from pure reagents: $K_2Cr_2O_7$ (ACS, Sigma-Aldrich), K_2CrO_4 (ACS, Merck), $Cr_2(SO_4)_3 \cdot nH_2O$ (RPE, Carlo Erba), $CrCl_3 \cdot 6H_2O$ (RPE, Carlo Erba), CrO_3 (ACS, Merck), Cr_2O_3 (99.9%, Merck). Chromite ($FeCr_2O_4$) reference material was purchased from Geostandards (Vandoeuvre Cedex, France). $Cr(OH)_3$ was prepared by precipitation with NaOH from a $CrCl_3 \cdot 6H_2O$ (RPE, Carlo Erba) solution. $CaCrO_4$ was obtained by a precipitation reaction between $CaCl_2 \cdot 2H_2O$ (RPE, Carlo Erba) and K_2CrO_4 (ACS, Merck). For both $Cr(OH)_3$ and $CaCrO_4$, the suspensions were centrifuged at 15.000 rpm for 15 minutes (SL16R Centrifuge, Thermo Scientific) and the collected precipitated material was freeze-dried with a liofilizer (Lyovapor L-200 Pro Büchi, Switzerland). All the Cr-reference compounds were diluted with BN (99%, Sigma-Aldrich) with an agate mortar and pestle in order to obtain a final concentration of 5% w/w of Cr. Finally, each standard mixture was pressed to obtain 20 mm diameter and 0.7 mm thickness tabs as described above.

Additional reference compounds were prepared by mixing $CrCl_3 \cdot 6H_2O$ (RPE, Carlo Erba) with different matrices: humic acids (EUROSOIL E5; Senesi et al., 2003), Compost (Progeva s.r.l., Italy), Goethite (α-FeOOH; Bayferrox 910-standard 86, Bayer; Terzano et al., 2010) and Illite (Illite #36 Morris, Illinois - Clay mineral standard).

About 50 mg of $CrCl_3 \cdot 6H_2O$ were dissolved in 10 ml deionized water and mixed with about 150 mg of each of the above-mentioned materials, maintaining the pH at 5.0-5.5 by adding 0.1 M KOH or HNO_3. The resulting suspensions were mixed for 12h with a magnetic stirrer and then centrifuged at 15.000 rpm for 15 minutes at 10°C; the supernatants were discarded, and the pellets were freeze-dried. Freeze-dried pellets were pulverized in an agate mortar and finally pressed to obtain 20 mm diameter and 0.7 mm thickness tabs, as described above.

2.5.1.2 Bulk XAS spectra acquisition

The energy calibration (Cr K-edge) was performed by using a pure metallic Cr foil. Cr XAS spectra were recorded by acquiring a total of 2400 points with an energy increment of ~ 0.6 eV in continuous mode in the energy range from 5839 eV to 6589 eV (-150 eV below to 600 eV above Cr-K edge) using a dwelling time of 0.05 s/point for a total of 120 s per spectrum.

XAS spectra of Cr reference compounds were recorded at ten different points on each tab, while twenty different points were measured in the case of samples. The acquired spectra for each tab were subsequently merged to improve the signal-to-noise ratio.

2.5.2 Microscopic-XANES analyses

The synchrotron X-ray microscopy measurements were performed at the Hard X-ray Micro/Nano-Probe beamline P06. Beamline P06 allows visualisation of various contrasts (XRF, XANES, XRD, ptychography) with micro- or nanoscopic spatial resolution using an energy range of 5-21 keV. The undulator radiation beam was monochromatized using a double Si(111) crystal monochromator (DCM) with an energy resolution of $\Delta E/E = 2 \cdot 10^{-4}$. For higher harmonic suppression, a pair of horizontally deflecting Si mirrors was used. The incoming beam was monitored by a 33 mm long ionization chamber filled with dry nitrogen. Afterwards, the beam was focused by a Kirkpatrick-Baez mirror system to a size (FWHM) of 370 x 800 nm^2 (h × w). The photon flux in the focus at the sample position was approximately 10^9 ph s^{-1} (Lutz et al., 2021), limited by air paths in the primary

beam. The beam hits the sample under 90°. The characteristic fluorescence radiation emitted from the sample was measured with a 50 mm^2 SII Vortex EM Si-drift detector (Hitachi High-Tech, Chatsworth/CA, USA) in 135° geometry. The 135° geometry was selected to minimize shading effects. The sample was mounted on a three-axis piezo scanner system (Aerotech, Pittsburgh/PA, USA) on top of an air bearing rotation stage and a hexapod (Newport, Irvine/CA, USA) for alignment. The piezo scanner system has a working range of 500 µm for every axis. A digital microscope equipped with the lens HV-Z50W (Keyence, Osaka, Japan) was installed between the sample and the Kirkpatrick-Baez mirror system to get a visual overview. A photograph of the set-up is shown in **Figure S1a**.

2.5.2.1 Soil thin section preparation

For microscopic XANES measurements, thin sections of the A2 sample heated at 500°C were prepared. The soil thin sections of 10 µm thickness were obtained after embedding the soil in epoxy resin, cutting and lapping with silicon carbide and diamond paste; soil thin sections were finally sealed with Kapton tape (3M) prior the analysis (**Figure S1b, S1c**).

2.5.2.2 Microscopic-XANES spectra acquisition

Lateral 2D element maps were collected by raster scanning the sample in continuous mode across the beam. Micro-XANES measurements were recorded by collecting lateral 2D XRF maps at various energies around the Cr-K absorption edge in fluorescence mode with continuous movement of the fast axes (sweep scan) and the energy as the third (slowest) axis. The energy of undulator and monochromator was scanned from 5980 eV to 6020 eV with 1 eV step size and Cr micro-XRF maps were acquired for each excitation energy setting a sampling step of 2 µm both horizontally and vertically (the horizontal axis was the fastest one) using an acquisition time of 5 ms for each lateral interval. In order to obtain the XANES spectrum of the whole analysed area, all the Cr maps acquired at each excitation energy were processed using the ROI imaging tool of PyMCA 5.6.5 (Solè et al., 2007) and a XANES sum spectrum of 41 energy channels was obtained. Then, to identify the areas where Cr(VI) was located, two regions of interest (ROI) of the spectrum were selected: total Cr was identified using the spectral region between 6016 eV and 6018 eV (see Section 3.5, mapped in red); while, the Cr(VI) characteristic pre-edge peak was mapped using the

ROI comprised between 5992 eV and 5994 eV (see Section 3.5, mapped in green). The ratio of the signal for "total Cr" and of the pre-edge region resulted in the identification of the areas containing Cr(VI) (Section 3.5, mapped in yellow).

The micro-aggregates where Cr(VI) was detected were further investigated with a higher lateral resolution XANES mapping using a stepsize of 0.4 μm (both horizontal and vertical with the horizonal axis set as the fastest one) and an energy range scanning from 5900 eV to 6200 eV with a step of 1 eV and an acquisition time of 5 ms per lateral step. Then, the same approach used for the other maps was applied to exactly identify the area containing Cr(VI) (see Section 3.5). After selecting the area containing Cr(VI) particles, the XANES spectrum was extracted and analysed (see Section 3.5). Possible photoreduction phenomena were checked by acquiring three spectra for each CrO_3 and $CaCrO_4$ standards. The calculated X-ray dose during the experiment was below 10^6 Gy. This preliminary check confirmed the reproducibility of the analysis and no photoreduction effect was observed (**Figure S2**).

2.5.3. Bulk XAS and micro XANES data processing

XAS spectra were processed by using Athena software included in Demeter 0.9.26 software (Ravel and Newville, 2005). All the spectra were calibrated for the energy, normalized, and clustered by using the principal component analysis (PCA). Chromium speciation in bulk soils as well as in soil thin sections was determined by linear combination fitting (LCF) using acquired reference compounds spectra and sample experimental data. The reduced Chi-square (χ^2) and the residual factor (R-factor) were used for primary goodness of fit assessment.

2.6 SEM-EDX analyses

Further investigations on soil thin sections were performed by means of field emission gun scanning electron microscopy coupled with microanalysis (FEGSEM-EDX, Zeiss Σigma 300 VP, Carl Zeiss NTS GmbH, Germany), to elucidate the chemical and micro/nano structural properties of soil aggregates with particular attention to Cr distribution. The instrument was equipped with an EDX C-MaxN SDD spectrometer with an active area of 20 mm^2 (Oxford Instruments) and operated at 15 kV at a working distance of 8.5 mm.

3. Results

3.1. Thermogravimetric analyses

The TGA curves with the corresponding first derivatives (i.e., Differential Thermogravimetry, DTG curves) of A1, A2 and Control soil samples are reported in **Figure 1a**, **1b** and **1c**, respectively. All the thermograms showed significant weight losses mainly in three intervals of temperature: i) at ca. 100°C, ii) between 200°C and 600°C, and iii) after 800°C. According to Terzano et al. (2021), it can be reasonably stated that in this kind of samples the weight loss in the first region is due to water evaporation, the thermal events in the second region are associated to the degradation of the organic matter, while decomposition of carbonates occurs in the third region. Based on these data, the temperatures of 300°C (DTG main peak of organic matter decomposition), 400°C (first inflection after the DTG main peak) and 500°C (first shoulder after the DTG main peak) were selected for the simulated thermal treatments, also considering the temperatures likely to be reached in fires occurring on agricultural soils (Li et al., 2012).

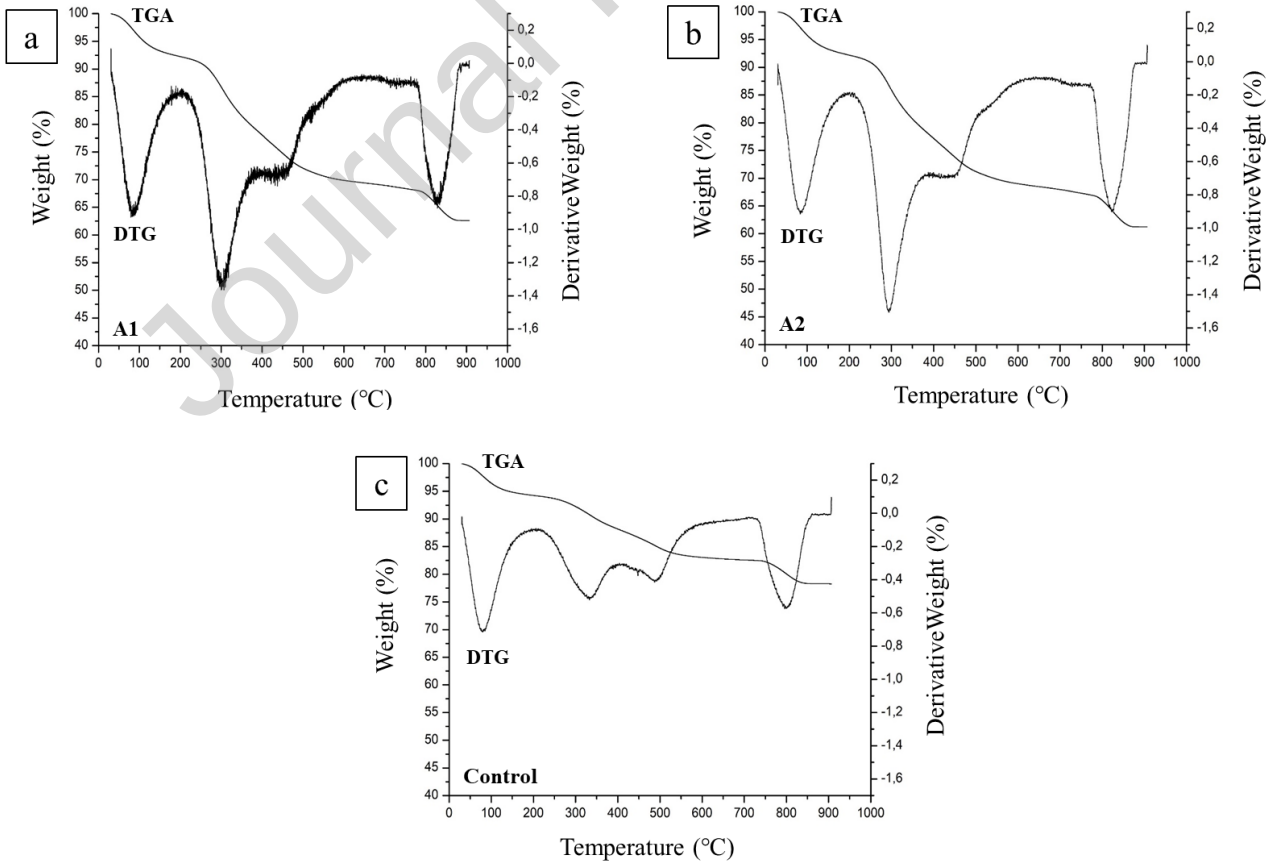

Figure 1: TGA and DTG curves of a) A1, b) A2 and c) Control soils showing the mass losses that occurred after heating samples from 30°C up to 900°C with a heating rate of 10°C min^{-1}.

3.2. Soil characterization at bulk scale

3.2.1. Chemical and mineralogical characterization of heated soils

Soil chemical analyses performed on Control, A1 and A2 soil samples heated up to 300°C, 400°C and 500°C revealed that the heating treatments significantly altered soil chemical properties compared to the unheated (N.T.) soils (**Table 1**). For all soil samples, pH increased with increasing temperatures, while E.C. strongly increased in 300°C-heated soils and then slightly decreased in soils heated at higher temperatures, although remaining much higher than in the unheated soils. The total $CaCO_3$ decreased in the Control soil with increasing temperatures, while it remained quite stable in the A1 and A2 polluted soils after the heating treatments. The active $CaCO_3$ fraction generally increased with the increasing temperature in the soils under investigation.

Organic C and total N content, as well as C.E.C. were strongly reduced after heating treatments, while available P increased with the increasing temperature.

The concentrations of base cations followed the sequence $Ca^{2+}>K^{+}\geq Mg^{2+}>Na^{+}$ in all the unheated soils, with a clear predominance of Ca^{2+} over the other bases, while after heating at 500°C the order changed in A1 and A2 soils becoming $Ca^{2+}> Mg^{2+}> K^{+}>Na^{+}$. The content of Ca^{2+} and K^{+} strongly decreased in all the soils under investigation with the increasing temperature, that of Mg^{2+} decreased or remained unchanged after the heating treatments, whereas Na^{+} concentration slightly increased.

The XRPD analysis performed on the soils before and after the thermal treatments did not reveal significant variations of the main mineralogical composition. As also reported by Gattullo et al. (2020), the main mineralogical phases are calcite, illite, quartz, and kaolinite. As an example, the diffractograms of the A2 sample, unheated and heated up to 300°C, 400°C and 500°C, are reported in **Figure S3**.

A detailed investigation of the diffraction peaks attributable to iron oxide minerals was carried out with a high-resolution diffractometer and the results for the region of interest are reported in **Figure S4**. In particular, the occurrence of a very small peak at about 35.4 2θ° in A2 400°C (green arrow) and a shift of the peak to higher 2θ° values in A2 500°C (blue arrow) was observed (**Figure S4**).

3.2.2. Chromium availability and fractionation

The total concentration of Cr slightly increased after thermal treatments (**Table 1**) due to OM depletion, while the Cr fraction potentially available for plants' uptake (assessed with DTPA extractions) strongly increased with increasing temperatures in the two polluted soils (A1 and A2), reaching values up to 108 and 106 mg kg^{-1} in A1 and A2 500°C-heated soils, respectively (**Figure 2a**).

Moreover, Cr fractionation, assessed by sequential extractions procedure (SEP), revealed that Cr distribution in heated soils (at 300°C, 400°C and 500°C) significantly changed compared to non-heated soils (A1 NT, A2 NT and control NT) (**Figure 3**). In particular, the percentage of Cr bound to the soil oxidisable fraction (bound to OM - Step 4 of SEP) strongly decreased with the increasing temperature, especially for the A1 and A2 soils. Conversely, the Cr associated to the soil residual fraction increased with the increasing temperature. In addition, an increase of the amount of Cr in soluble or exchangeable forms (Step 1 of SEP) was also observed with the increasing temperature with values up to 119 and 124 mg kg^{-1} in A1 and A2 polluted soils, respectively (**Figure 2b**). Such a trend and concentrations are similar to those of Cr extracted with DTPA (**Figure 2a**).

Table 1: Chemical properties of the polluted (A1 and A2) and unpolluted (Control) soils before (N.T.) and after laboratory-heating simulations (300°C, 400°C and 500°C). Data are reported as mean ± standard deviation (n=3).

		CONTROL				A1				A2			
		N.T.	**300**	**400**	**500**	**N.T.**	**300**	**400**	**500**	**N.T.**	**300**	**400**	**500**
pH (KCl)		7.3 ± 0.1	7.1 ± 0.1	8.1 ± 0.1	7.6 ± 0.1	7.2 ± 0.1	7.7 ± 0.2	8.1 ± 0.1	8.2 ± 0.1	7.1 ± 0.1	7.7 ± 0.1	8.0 ± 0.1	8.2 ± 0.1
E.C. (mS cm^{-1})		0.13 ± 0.01	2.80 ± 0.19	2.07 ± 0.16	1.84 ± 0.08	0.21 ± 0.30	4.15 ± 1.59	3.10 ± 1.01	3.51 ± 0.23	0.24 ± 0.03	4.37 ± 0.49	2.93 ± 0.96	2.63 ± 0.74
C.E.C. ($cmol_{(+)}/kg$)		50.8 ± 5.8	36.6 ± 1.3	27.4 ± 1.2	19.8 ± 3.0	75.1 ± 7.5	37.3 ± 3.8	33.5 ± 3.4	27.5 ± 3.5	76.2 ± 10	42.1 ± 6.7	37.4 ± 4.4	32.6 ± 4.3
Total $CaCO_3$ (g kg^{-1})		165.7 ± 11	93.2 ± 11	87.7 ± 9.2	82.5 ± 6.5	196.1 ± 16	201.6 ± 26	200.8 ± 22	210.9 ± 24	202.4 ± 17	234.4 ± 26	233.7 ± 16	240.4 ± 30
Active $CaCO_3$ (g kg^{-1})		13.6 ± 1.2	10.3 ± 3.1	20.3 ± 1.4	18.7 ± 1.3	75.1 ± 10.3	87.7 ± 0.4	110.1 ± 5.1	115.5 ± 14.	116.4 ± 16	76.8 ± 1.9	136.3 ± 1.2	149.1 ± 4.4
Organic Carbon (OC) (g kg^{-1})		48.8 ± 6.5	33.7± 3.3	17.5 ± 1.7	6.5 ± 0.8	124.6 ± 16	72.6 ± 18	35.7 ± 10	17.4 ± 3	135.9 ± 20	61.3 ± 6.9	38.5 ± 1.5	18.0 ± 3.2
Organic matter (OM) (%)		8.4 ± 1.1	5.8 ± 0.6	3.0 ± 0.3	1.1 ± 0.1	21.5 ± 2.8	12.5 ± 3.1	6.2 ± 1.8	3.0 ± 0.5	23.4 ± 3.5	10.6 ± 1.2	6.6 ± 0.3	3.1 ± 0.5
Total N (g kg^{-1})		3.9 ± 0.5	3.4 ± 0.2	2.6 ± 0.2	1.0 ± 0.1	13.1 ± 1.2	9.4 ± 0.4	5.4 ± 0.7	2.4 ± 0.2	15.0 ± 1.5	10.9 ± 1.0	6.2 ± 0.4	2.5 ± 0.2
Available P (mg kg^{-1})		4.6 ± 0.2	95.4 ± 5.3	83.2 ± 6	48.4 ± 8.5	98.2 ± 11	160.2 ± 10	223.2 ± 27	282.0 ± 2.1	182.8 ± 24	184.9 ± 9.3	243.0 ± 21	397.1 ± 44
Exchangeable bases	**Ca^{2+} ($cmol_{(+)}$ kg^{-1})**	28.4 ± 1.9	19.3 ± 1.2	20.2 ± 7.3	11.8 ± 2.7	45.4 ± 4.7	25.7 ± 4.8	32.0 ± 0.6	33.7 ± 1.6	48.3 ± 3.8	30.2 ± 1.4	35.5 ± 1.6	38.9 ± 1.9
	Mg^{2+} ($cmol_{(+)}$ kg^{-1})	1.1 ± 0.1	0.7 ± 0.1	0.6 ± 0.2	0.8 ± 0.1	1.9 ± 0.4	1.06 ± 0.3	1.5 ± 0.5	1.3 ± 0.3	2.0 ± 0.3	1.6 ± 0.6	1.9 ± 0.6	1.8 ± 0.5
	Na^{+} ($cmol_{(+)}$ kg^{-1})	0.10 ± 0.01	0.36 ± 0.03	0.28 ± 0.13	0.31 ± 0.15	0.10 ± 0.01	0.31 ± 0.01	0.29 ± 0.06	0.19 ± 0.07	0.10 ± 0.02	0.41 ± 0.01	0.40 ± 0.05	0.27 ± 0.07
	K^{+} ($cmol_{(+)}$ kg^{-1})	1.9 ± 0.4	1.7 ± 0.3	1.4 ± 0.1	1.1 ± 0.3	2.4 ± 0.6	1.1 ± 0.3	1.2 ± 0.1	0.8 ± 0.1	2.2 ± 0.4	1.3 ± 0.3	1.1 ± 0.2	0.8 ± 0.1
Total Cr (mg kg^{-1})		65 ± 11	59 ± 8	53 ± 2	46 ± 6	3807 ± 30	4123 ± 77	4039 ± 72	4284 ± 21	5185 ± 35	5397 ± 81	6246 ± 111	5715 ± 13

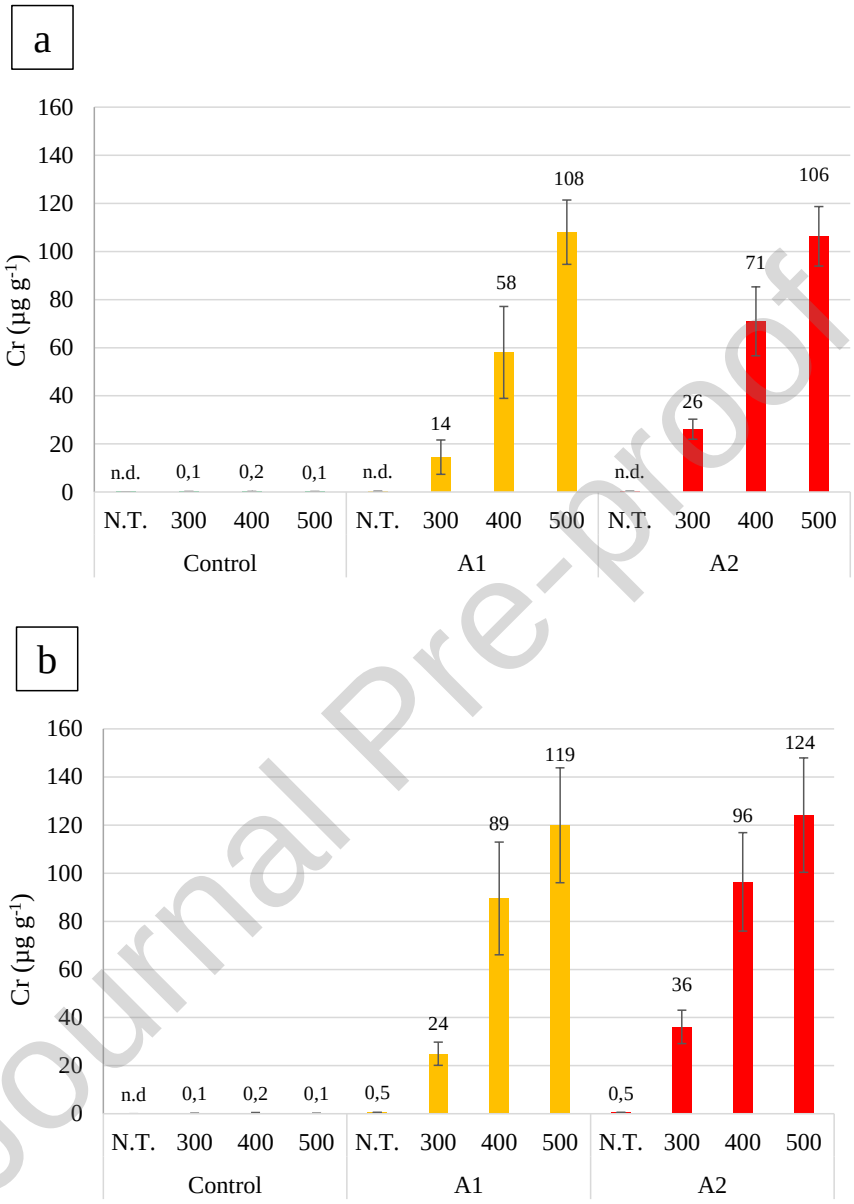

Figure 2: (a) Cr-DTPA extractable fraction and (b) Cr in soluble or exchangeable forms (Step 1 of SEP). n.d.: not detectable

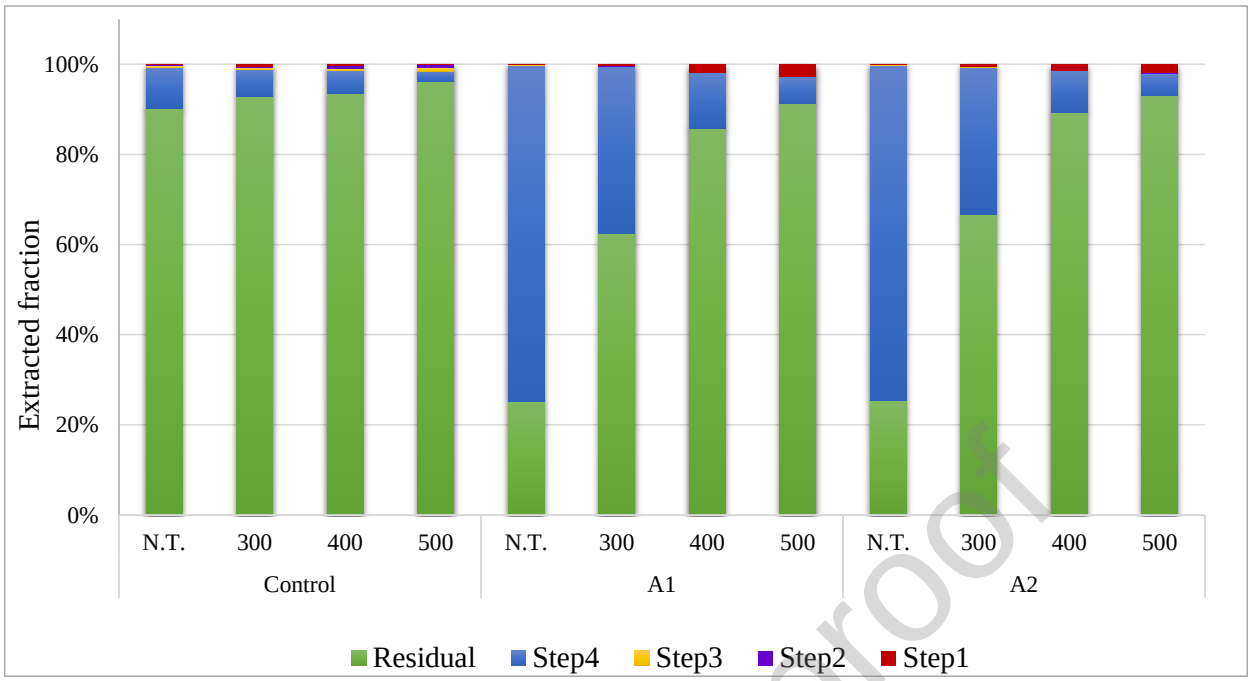

Figure 3: Cr fractionation in Control, A1 and A2 soils, before (NT) and after laboratory heating simulations (300°C, 400°C and 500°C); Step 1 ($MgCl_2$): Soluble and exchangeable fraction; Step 2 (CH_3COOH): Carbonates bound and acid soluble fraction; Step 3 (NH_2OH HCl): Reducible fraction (bound to Fe and/or Mn oxides); Step 4 (H_2O_2 + HNO_3): Oxidisable fraction (bound to OM); Residual fraction: recalcitrant fraction present in the soil at the end of the 4th step.

3.2.3. Hexavalent chromium determinations

Total Cr(VI) content in the two polluted soils (A1 and A2) increased with increasing temperature, reaching values considerably higher than the Italian national regulatory threshold for agricultural sites (2 mg kg^{-1}; Italian Legislative Decree n.152/2006) (**Figure 4a**).

An increase of exchangeable Cr(VI) content with increasing temperatures was also observed and the highest values were observed for the A1 and A2 soil samples treated at 400 and 500°C, reaching about 30-40 mg kg^{-1} (**Figure 4b**). Between 20% and 90% of the total Cr(VI) content was in the exchangeable form, depending on heating temperature. Neither Cr(VI), nor exchangeable Cr(VI) were detected in the Control soil with increasing temperature and in the polluted not-heated soils (**Figure 4a, 4b**).

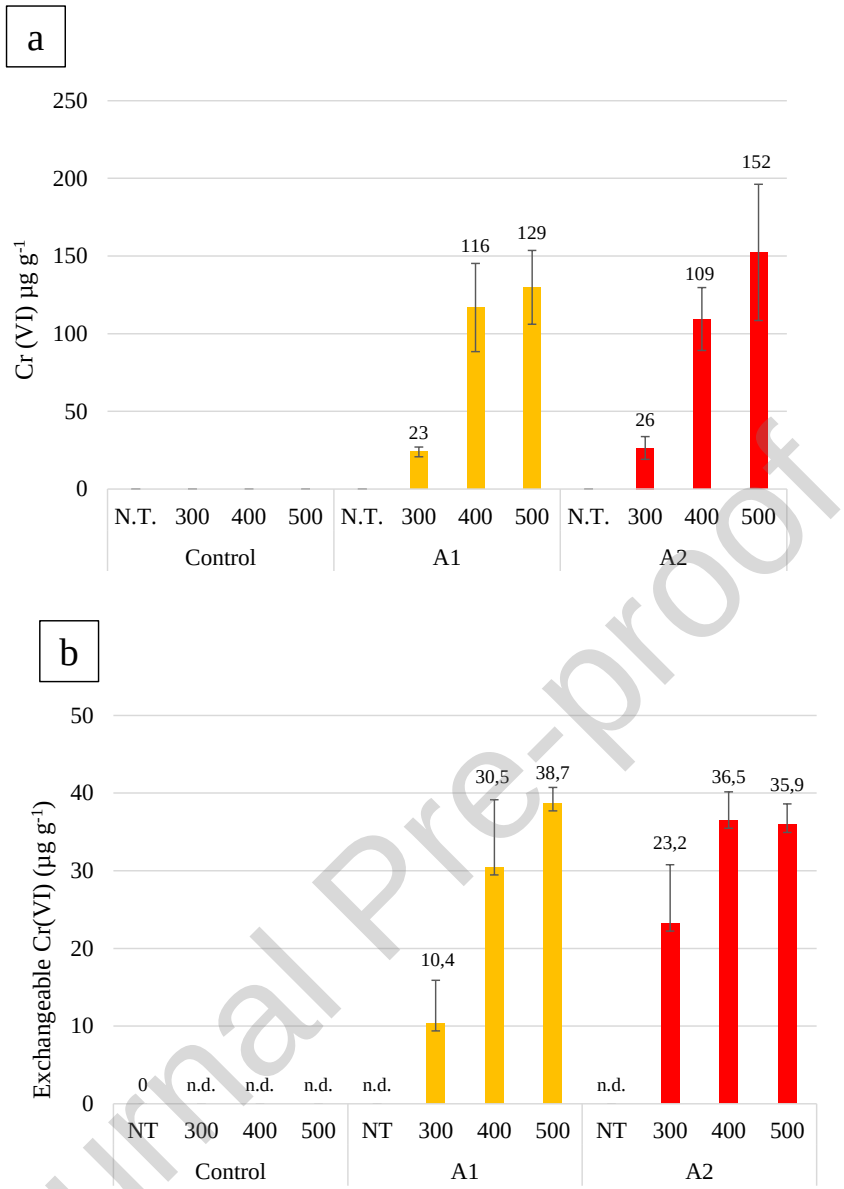

Figure 4: (a) Total Cr(VI) and (b) exchangeable Cr(VI) concentrations in A1, A2 and control soils before (NT) and after laboratory heating simulation. n.d.: not detectable

3.3. Chromium distribution at the micro-scale: µ-XRF

The analysis performed by means of laboratory µ-XRF revealed that Cr within soil aggregates was mostly correlated to Fe (main trend corresponding to the green region of the scatterplot and green particles in the map, **Figure 5a**) and Ca (two principal trends corresponding to the cyan and green regions of the scatterplot, and the cyan and green particles in the maps, **Figure 5b**). These correlations remained unchanged over the heating experiments, as can be observed, for example, by comparing the A2 NT with the A2 500 °C correlation maps in **Figure 5a** and **5b**. In A2 300 °C and

A2 400 °C, the same correlations were identified (data not shown). Moreover, aggregates dimension became smaller with increasing temperature, as shown by the histogram in **Figure 5c**.

In particular, it was observed that in the A2 NT soil the most frequent major diameter of Cr-Ca-Fe containing aggregates was in the 640-1280 µm range, while after the heating treatment at 500 °C it decreased to the 320-640 µm range (**Figure 5c**).

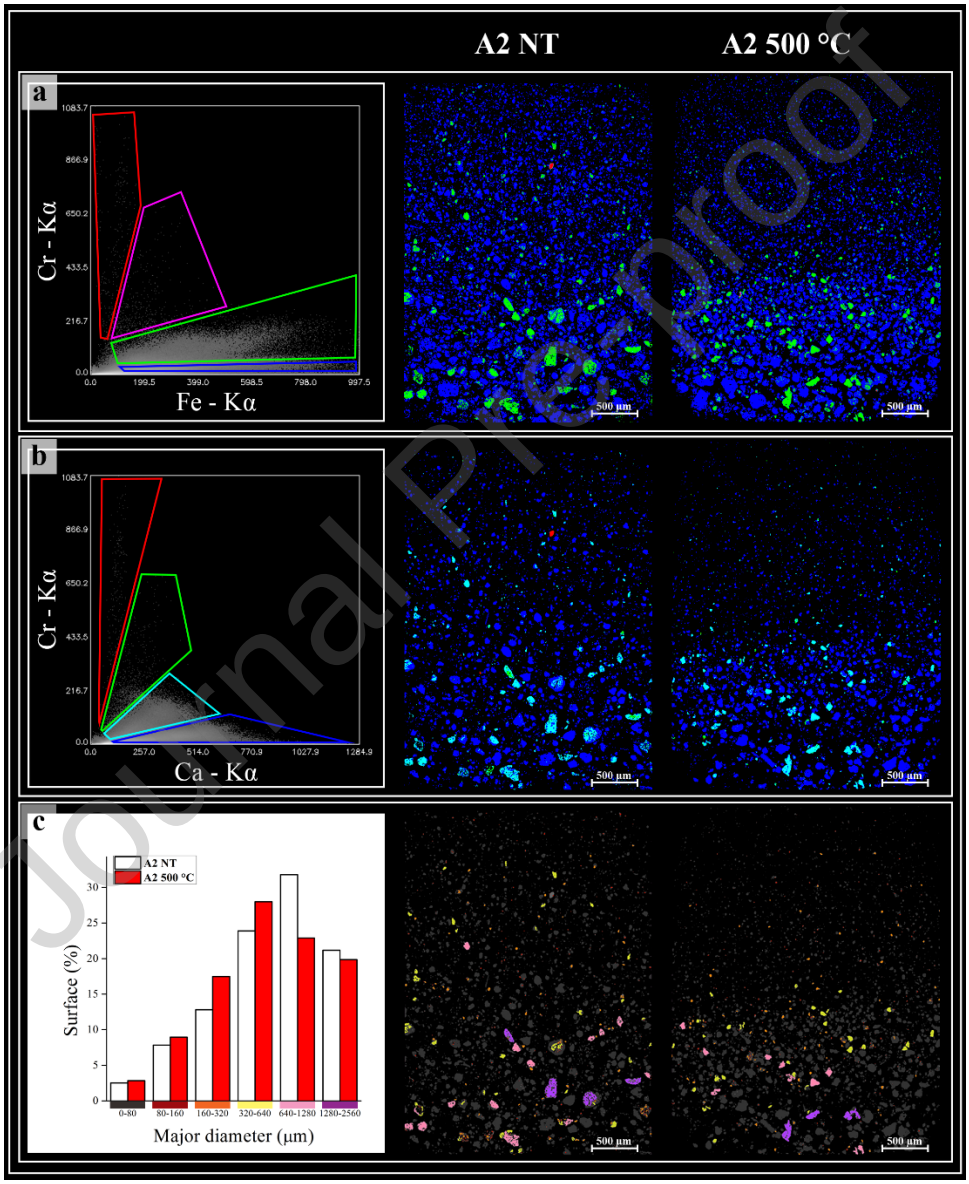

Figure 5: a-b, right panels) µ-XRF distribution maps of soil thin sections of the A2 sample treated at 500°C (A2 500 °C) or not-treated (A2 NT). A2 NT and A2 500 °C maps in a) and b) are coloured on the basis of the trends (coloured boxes) identified within the scatterplots shown on the left panel reporting a) the Fe and Cr Kα-lines intensities correlation and b) the Ca and Cr Kα-lines intensities correlation, respectively.

c, left panel) Histogram showing the size distribution of soil aggregates containing Cr-Ca-Fe: each dimensional range is colour-coded and used to recolouring the µ-XRF maps (right panels) to visualize particle-size distribution on the thin sections.

3.4. Chromium speciation: bulk XAS

Chromium XAS spectra of Cr(III) and Cr(VI) reference compounds are reported in **Figure 6**. In particular, the pre-edge peak (5993 eV), which is characteristic of Cr(VI), was clearly detected in all Cr(VI) reference materials (CrO_3, $K_2Cr_2O_7$, K_2CrO_4, $CaCrO_4$). Beside reference materials, Cr XAS spectra were collected only for the A2 soil sample, being the sample with the highest Cr concentration and therefore more suitable for XAS analyses. XAS spectra of the A2 sample not treated (NT) or treated at 300, 400 and 500°C are shown in **Figure 7**. It can be observed that the XAS spectra changed with increasing temperatures, suggesting a change in Cr speciation. However, no pre-edge peak was detected in the bulk XAS spectra of the investigated soils. Indeed, according to the data presented in the previous sections, in A2 samples Cr(VI) was below 3.5% of total Cr, which is below the detection limit of XAS, usually in the order of 10-15% of the total element concentration (Terzano et al., 2008).

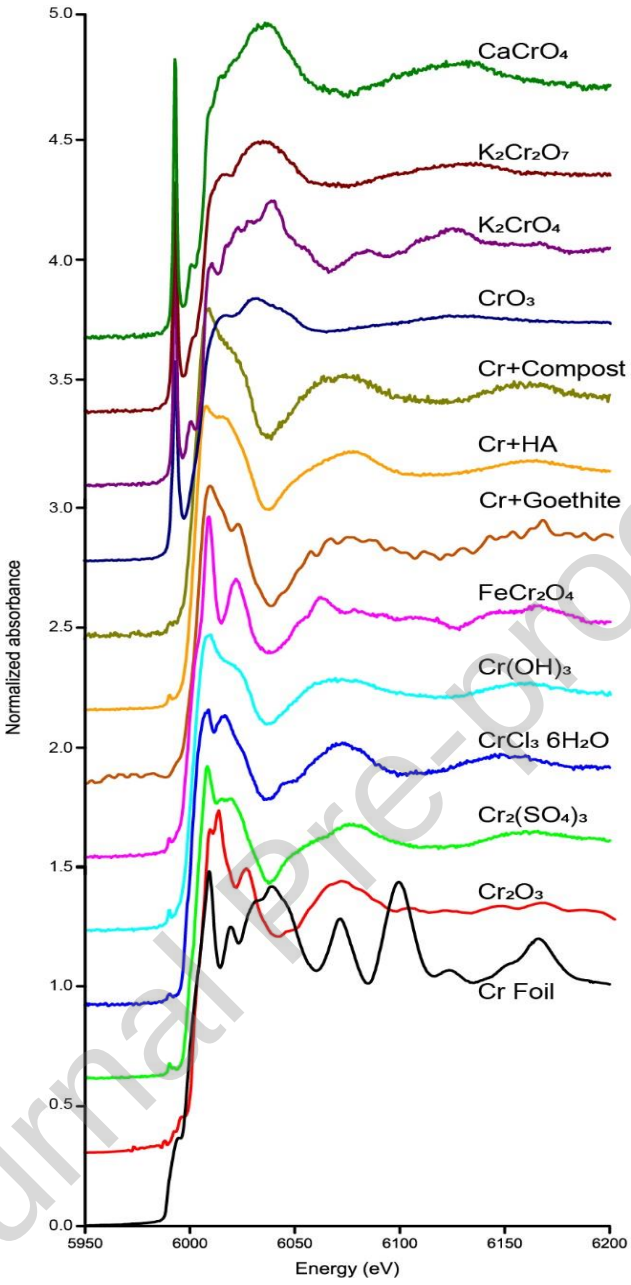

Figure 6: Cr XAS spectra of Cr(III) and Cr(VI) reference compounds.

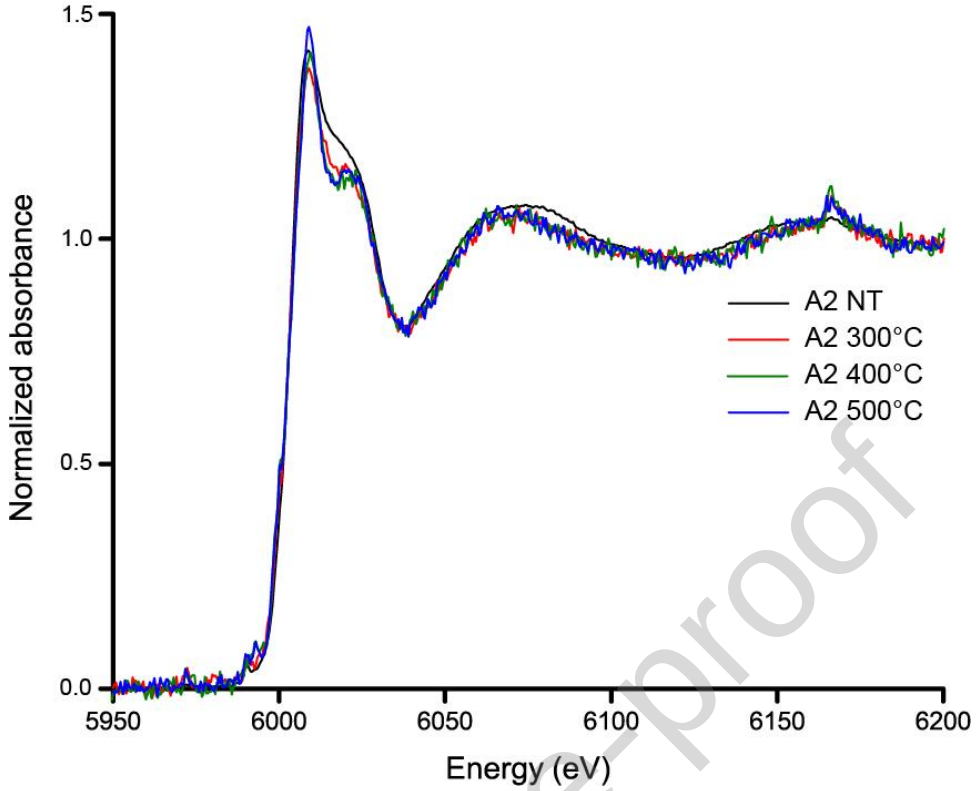

Figure 7: Cr XAS spectra of A2 soils either unheated (A2 NT) and after heating up to 300°C, 400°C and 500°C.

The XANES region of Chromium XAS spectra of A2 soils was fitted using the XAS spectra acquired for Cr-reference compounds and the linear combination fitting (LCF) results are shown in **Figure 8**. According to these data, in the unheated soil (A2 NT), Cr was mainly present in two forms: Cr(III)-compost (88%) and Cr(III)-goethite (12%) (**Figure 8a**). Cr(III)-compost percentage strongly decreased with the increasing temperature (from 88% in the unheated soil to about 38% in the A2 soils treated at 400 (**Figure 8c**) and 500°C (**Figure 8d**)). Conversely, Cr(III)-goethite content increased from 12% in the A2 NT soil (**Figure 8a**) up to 43% in the A2 300°C-heated soil sample (**Figure 8b**). Then, at increasing temperatures (A2 400°C and A2 500°C), a slight decrease of Cr(III)-goethite percentage was observed, reaching about 35% at 500°C (**Figure 8c**,**8d**).

In addition, the formation of chromite ($FeCr_2O_4$) was observed in all the heated samples and its percentage increased with increasing temperature from about 12% at 300°C to 27% at 500°C.

The quality of the fitting was confirmed by the low values of both reduced Chi-square (Red χ^2) and residual factor (R-factor).

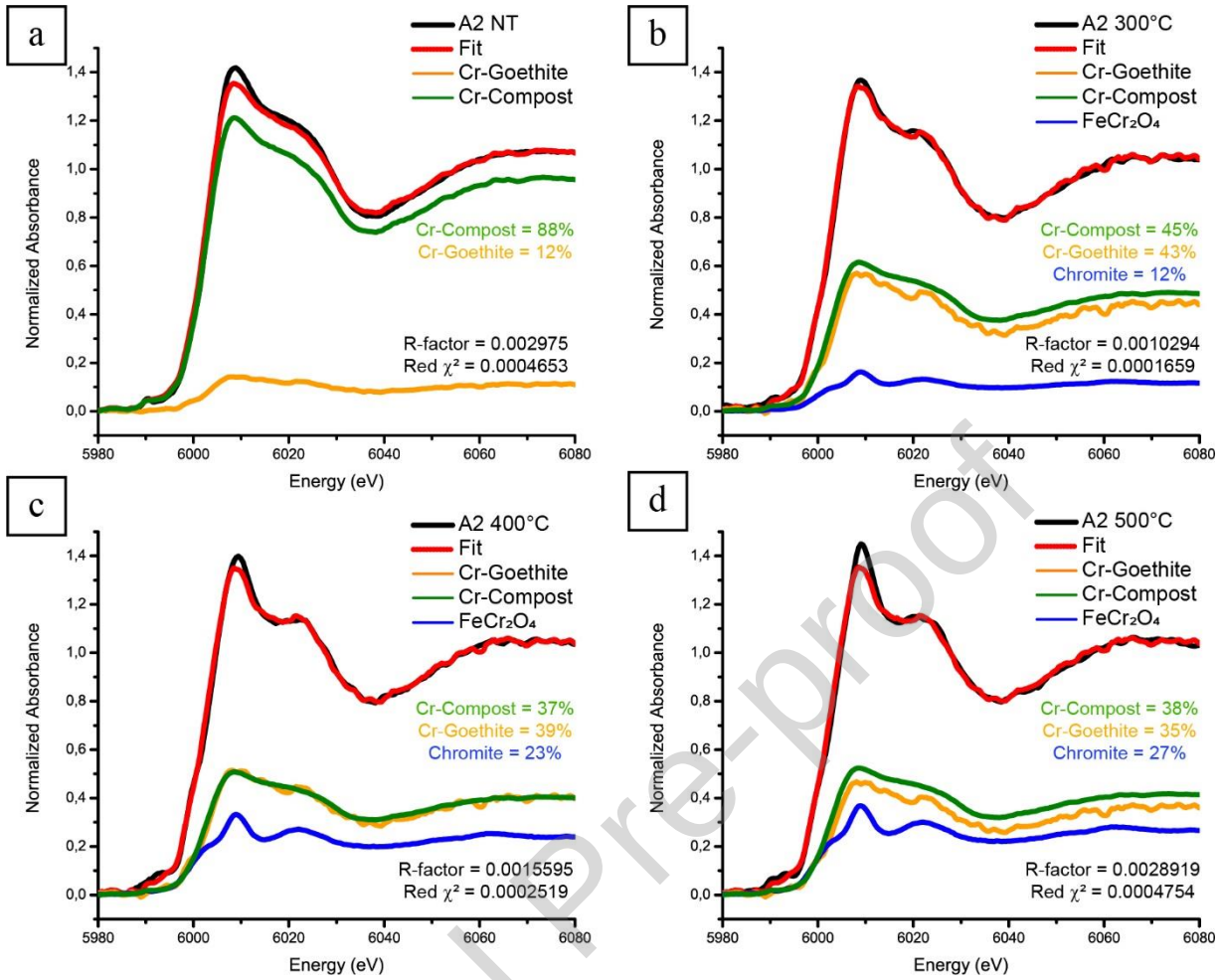

Figure 8: Results of the LCF performed on Cr XAS spectra acquired from A2 bulk soils both before (A2 NT) a) and after laboratory-heating simulations up to 300°C b), 400°C c) and 500°C d).

3.5. Chromium speciation: Micro-XANES mapping

A2 soil sample treated at 500°C was additionally studied by µ-XANES imaging, being the sample with the highest Cr(VI) concentration. Indeed, µ-XANES mapping allowed to identify very few microscopic regions of the sample (about 20-50 μm^2) containing Cr(VI) forms (**Figure 9**). The Cr-distribution map reported in **Figure 9a** shows in red the pixels were Cr is present, with no distinction between Cr(III) and Cr(VI) forms. In **Figure 9b** and **9c** red indicates Cr(III) while the addition of yellow pixels represent the areas where both Cr(III) and Cr(VI) are present. The Cr(VI) distribution maps (**Figure 9b** and **9c**) were obtained by recording the intensity of the characteristic pre-edge peak (measured between 5992 and 5994 eV) as a function of the position on the soil thin section (**Figure 9d**).

A higher resolution map was collected in the region containing Cr(VI) (**Figure 9c**) and a sum spectrum of all the pixels contained in that area was obtained (**Figure 9e**).

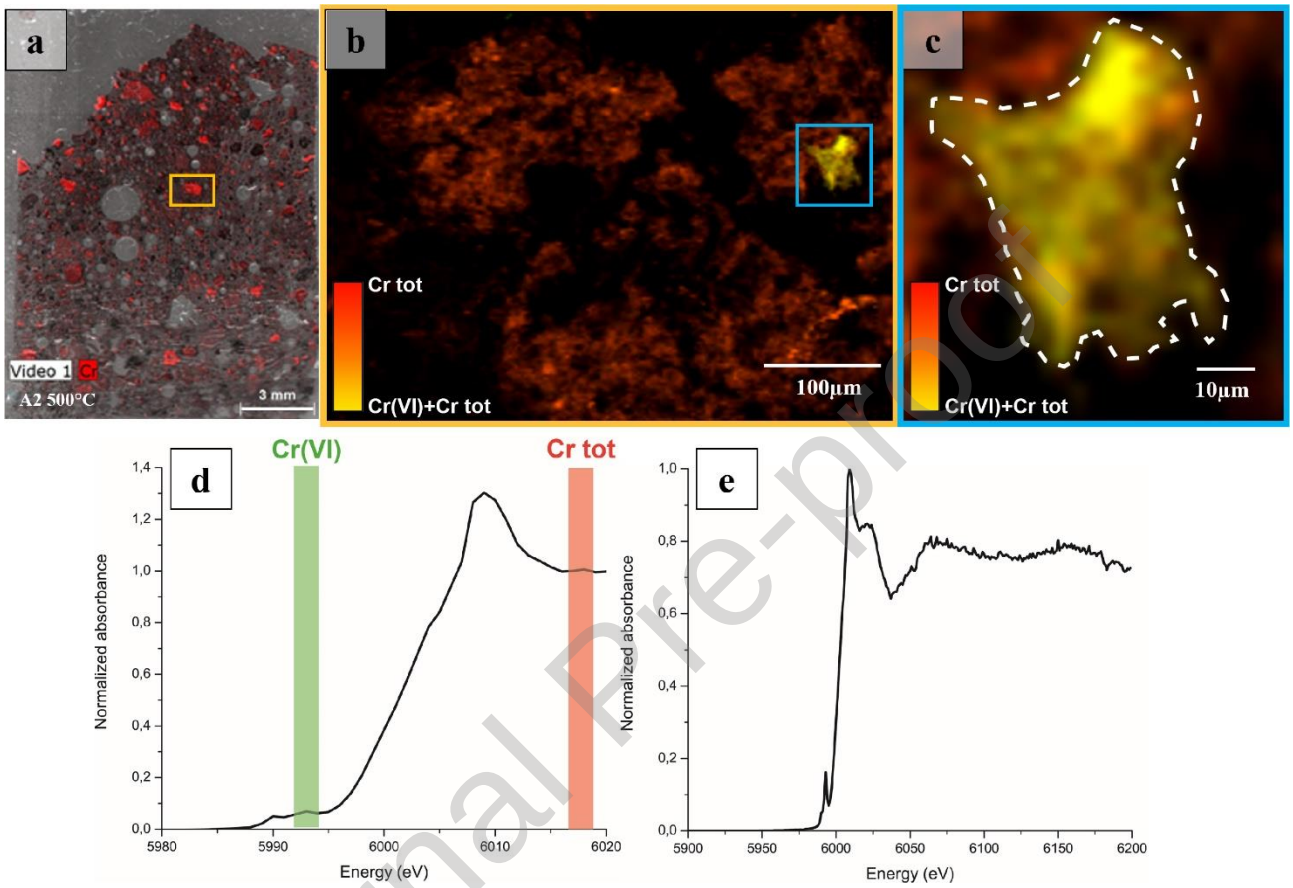

Figure 9: (a) Micro XRF Cr-distribution map (red pixels) over a thin section of the A2 500°C-heated soil acquired with M4 TORNADO. The yellow rectangle in (a) marks the region within which µXANES mapping was performed. (b) µXANES mapping of part of the yellow-bordered area in (a). (c) Cr-µXANES mapping performed at higher resolution of the area marked with the cyan rectangle in (b). Red pixels show total Cr distribution while yellow pixels Cr(III)+Cr(VI) distribution. (d) Cr-XANES spectrum of the µXANES map in (b). The ROIs of the total Cr (red) and of the characteristic Cr(VI) pre-edge peak (green) are also reported. (e) Cr-XANES spectrum of the complete map in (c). The white dashed line identified the area from which the spectrum shown in Figure 10 is extracted.

This sum spectrum was fitted using the XANES spectra of Cr(III) and Cr(VI) reference compounds (**Figure 10**). The LCF revealed the presence of three Cr forms: Cr(III)-goethite (46%), chromite (24%), and the Cr(VI) compound $CaCrO_4$ (30%) (**Figure 10**).

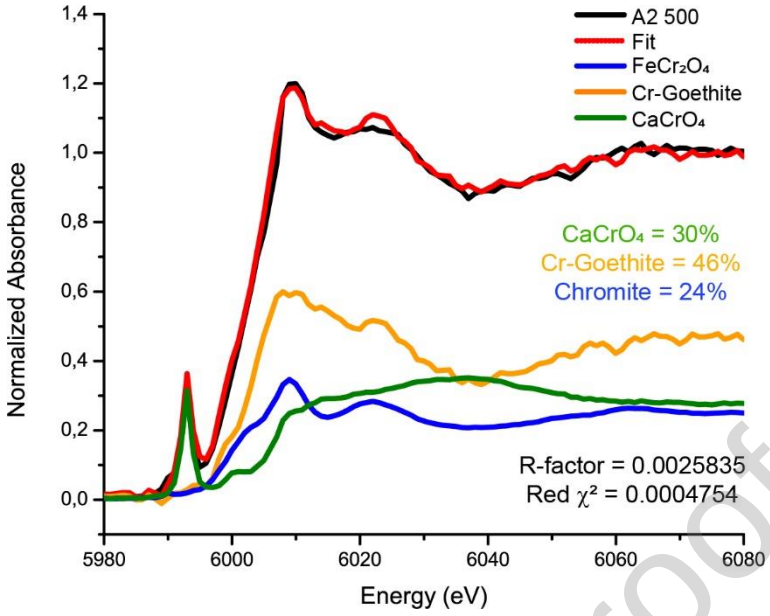

Figure 10: Results of the LCF performed on the Cr µXANES spectrum acquired from the Cr(VI)-containing area (identified by the white dashed line) of Figure 9c.

3.6. Cr distribution at the submicrometric scale: FEGSEM-EDX

Additional FEGSEM-EDX analyses were performed on A2 500°C soil thin section to assess the distribution of Cr at the submicrometric scale. In particular, the same Cr-containing aggregate studied with µ-XANES, was investigated. The high definition back scattered detector (HDBSD) micrograph (**Figure 11a**) showed the microstructure of the analysed area.

The elemental analysis performed with FEGSEM-EDX revealed the presence of Ca-rich and Fe-rich domains in the area where Cr(VI) was detected. Association of Cr, Ca and Fe are particularly evident in the particle indicated by the yellow arrow in **Figure 11b**.

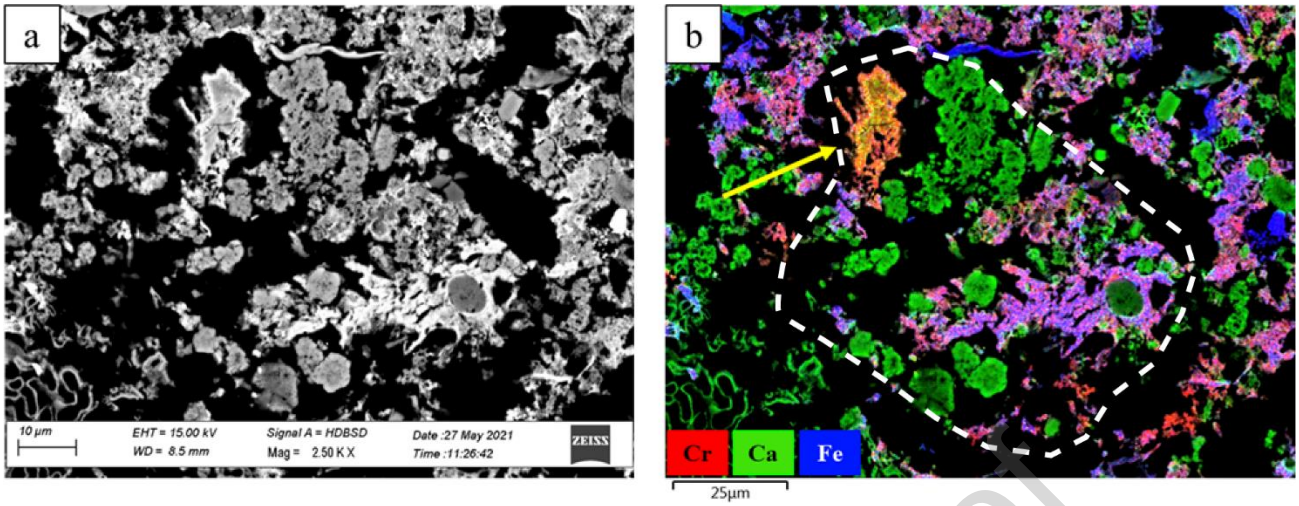

Figure 11: (a) High definition back scattered detector (HDBSD) image of the area shown in **Figure 9c** and analysed by µXANES. (b) FEGSEM-EDX elemental distribution of Cr, Ca and Fe. The area surrounded by the white dashed line corresponds approximatively to the yellow area in **Figure 9c** (slightly rotated). Different colours in (b) correspond to different degrees of overlapping of Cr (red), Ca (green) and Fe (blue).

4. Discussion

Thermogravimetric analysis data provided information on the thermal behaviour of the soil samples. In particular, the TGA/DTG curves (**Figure 1**) showed characteristic trends due to mass losses phenomena. At temperatures below 150-200 °C, the mass loss is mainly due to the loss of water by vaporization (Chandler et al., 1983) as well as the initial degradation of large organic molecules like lignin and hemicellulose (Rabenhorst, 1988); in the range 200°C–600°C, the mass loss can be mainly attributed to the thermal decomposition of organic matter, until almost complete consumption (Giovannini et al, 1990). In addition, the peak (Control) or shoulder (A1 and A2) at about 500°C could also be attributed to the dehydroxylation of clay minerals, in particular illite (Earnest, 1991a) and kaolinite (Lee et al., 1999), which in these soils accounted for about 20% and 8%, respectively (Gattullo et al., 2020). Finally, in the range 700°C-950°C the mass loss is probably attributable to the dehydroxylation of metallic hydroxides and to the calcination of carbonates (Plante et al., 2009; Giovannini et al., 1990), the second being more relevant since carbonate content in the soil samples was about 15-20%. Based on thermogravimetric data, three thermal ramps (up to 300°C, 400°C and 500°C) were selected for laboratory-simulated fires.

After the heating treatments, soil pH increased with increasing temperature (**Table 1**) as a consequence of the loss of organic acids, the release of oxides, hydroxides, carbonates and cations through ash particles, and the displacement of H^+ from the exchange sites by base cations (Terzano et al., 2021; Terefe et al., 2008; Certini, 2005). The increase of EC with the increasing temperature

(**Table 1**) was probably due to the release of soluble inorganic ions deriving mainly from the combustion of OM, but also from the exchange complexes (Terefe et al., 2008).

Soil CEC decreased consequently to the loss of high-density negatively charged fractions, mainly OM (Certini, 2005). The latter in fact decreased of about 80-90% at the highest temperatures of treatment (**Table 1**). It is known that OM can experience different alteration processes with increasing temperatures, ranging from the degradation of lignin and hemicellulose (130°C-200°C), to substantial combustion (200°C-300°C), accumulation of aromatic compounds (250°C-460°C), up to the almost complete decomposition which occurs at about 500°C (Giovannini et al., 1990). Nevertheless, approximately 3% of OM still remained in A1 and A2 soils after heating at 500°C. A more prolonged burning treatment is evidently required to degrade completely OM in highly organic soils.

Concomitantly with OM decrease, total nitrogen content decreased at increasing burning temperatures being more than 90% of total N in the organic form. The Kjeldahl method here adopted to measure the total N does not determine the nitric forms. Therefore, a release of NO_3^- after soil burning cannot be excluded, but its potential contribution to the overall soil properties would be very limited due to the rapid leaching of nitrate in soil.

The OM decomposition favoured the release of inorganic phosphorous, as proved by the increase of the available P concentration with the increasing temperature (**Table 1**). Burning processes in fact can convert the organic phosphorous pool into orthophosphate which is the most available P form for soil biota (Certini, 2005).

Total carbonate content in both polluted soils slightly varied with the increasing temperature (**Table 1**), in agreement with findings reported by Abraham et al. (2018). Conversely, active $CaCO_3$, which is the finest and most reactive carbonate fraction, increased with increasing temperatures (del Campillo et al., 1992). This outcome is most likely connected to the reduction of soil particle size after burning.

The concentrations of base cations after soil heating at 500°C followed the sequence Ca^{2+}> Mg^{2+}> K^+>Na^+ in A1 and A2 soils, and Ca^{2+}>K^+> Mg^{2+}>Na^+ in the control soil. As expected, the concentration of exchangeable bases decreased with the increasing temperature, concomitantly with C.E.C decrease, except for Na^+. No matches were found with other literature studies concerning the observed increase of exchangeable Na^+. However, Guerrero et al. (2005) observed a slight increase

of available Na in a forest soil after different thermal treatments up to 700°C. The absolute content of exchangeable Ca^{2+} decreased with increasing temperature, and possibly a fraction of calcium precipitated as Ca-phosphate (Badìa and Martì, 2003).

The effect of fire on mineral components can vary significantly according to soil characteristics (water and OM content, porosity, redox environment, etc.) as well as to fire magnitude in terms of temperature and residence time (Terzano et al., 2021). As observed by XRPD analysis (**Figure S3**), no significant changes of the main mineralogical composition occurred after thermal treatments. This evidence could be explained by considering that the mineralogical assemblage is generally altered at temperatures over 550°C, at which the first step of disruption of most minerals (dehydroxylation) occurs (Certini, 2005). Consequently, it might be possible that the selected thermal ramps (up to 300°C, 400°C and 500°C) were not high enough to cause significant mineralogical transformations. The analysis performed by means of high-resolution diffractometry (**Figure S4**) revealed small variations in the range 35-36 2θ°, with the appearance of a small peak at 35.4 2θ° in A2 400°C and a shift of the peak to 35.8 2θ° in A2 500°C. This peak could be attributed to the most intense diffraction line (113) of maghemite, magnetite or chromite. These phases have a very similar XRPD pattern and their discrimination cannot be done only based on their main peak. As reported by Cudennec and Lecerf (2005) and Ketterings et al. (2000), maghemite crystallization may occur when heating iron oxides in presence of OM; OM may also trigger the formation of maghemite after magnetite formation in the thermal range between 227 and 400°C (Terzano et al., 2021). The progressive transformation of goethite to maghemite upon burning of organic-rich, goethite-bearing soils was observed by Johnston et al. (2019), Ketterings et al. (2000), and Grogan et al. (2003). Moreover, as the soil under investigation contained high Cr concentrations, it is also possible to hypothesize the formation of chromite-like spinel mineral structures (Terzano et al., 2007). In fact, due to its charge and similar ionic radius, Cr(III) can substitute Fe(III) in Fe(III)-(oxy)hydroxides (Burton et al., 2019a).

Chromium total concentration slightly increased after thermal treatments (**Table 1**) as a consequence of OM mineralization. Chromium DTPA extractable fraction (potentially bioavailable fraction, **Figure 2a**) as well as Cr fractionation (**Figure 3**), were markedly influenced by the increasing temperature.

Specifically, Cr DTPA-extractable fraction strongly increased with the increasing temperature in both A1 and A2 soils (**Figure 2a**). Moreover, Cr fractionation revealed that, while in the unheated

A1 and A2 soils Cr was almost completely bound to OM, after the thermal treatments this fraction dramatically decreased with the increasing temperature due to OM mineralization. Conversely, the percentage of Cr in the residual fraction strongly increased by almost the same extent after the thermal treatments (**Figure 3)**. The soluble and exchangeable fraction (Step 1 of SEP) also increased with the increasing temperature (**Figure 2b**). In this regard, the depletion of OM as well as the increase of soil salinity, might have favoured Cr mobility due to the decrease of sorption sites and competition with salt derived ions (Acosta et al., 2011). A similar increase of the residual as well as the exchangeable and acid-soluble soil fractions was observed by Nordmark et al. (2011) after treating at 800°C for 20 min soil samples highly contaminated by Cr, As and Cu.

Laboratory-simulated fires caused also the partial oxidation of Cr(III) to Cr(VI), in agreement with other studies (Panichev et al., 2008; Burton et al., 2019b). These authors demonstrated that the Cr oxidation process can be favoured by the presence of carbonates, either released by fuel combustion or present in the soil itself, and/or by Fe (oxy)hydroxides transformation after thermal treatments. The total Cr(VI) content increased with the increasing temperature (**Figure 4a**) and an amount of the total Cr(VI) comprised between 20-30%, after treatments at 400-500°C, and 45-90%, after the treatment at 300°C, was exchangeable (**Figure 4b**). Indeed, exchangeable Cr(VI) increased with the increasing temperature and the highest values were observed after heating at 400°C and 500°C both A1 and A2 soils, in accordance with the findings of Burton et al. (2019b).

Total Cr(VI) and exchangeable Cr(VI) values were considerably higher than the safety threshold limits established for agricultural sites in Italy (2 mg kg^{-1}; Italian Legislative Decree n. 152/2006) thus underlying their potential hazardousness.

Nevertheless, the Cr(VI) concentrations measured were below the detection limit of bulk XAS analysis, but they could be detected by µXAS (**Figure 7**, **Figure 9**).

Chromium speciation assessed by bulk XAS revealed that in unheated soils (A2 NT) Cr was mainly present in two forms: Cr(III)-compost (88%) and Cr(III)-goethite (12%) (**Figure 8a**). Cr(III)-compost percentage strongly decreased with the increasing temperature (from 88% in the unheated soil to about 38% in the A2 soils treated at 400 and 500°C) (**Figure 8**) in accordance with the above discussed OM depletion with increasing temperature (**Table 1**). Conversely, Cr(III)-goethite content increased from about 10% in the A2 NT soil up to 43% in the A2 300°C-heated soil sample and then slightly decreased with increasing temperature reaching about 35% at 500°C (**Figure 8**). An increase of chromite ($FeCr_2O_4$) was also observed in all the heated samples (from 11% at 300°C

up to 26% at 500°C) (**Figure 8**). The increase of Cr(III)-goethite and chromite content might be related to Cr-mobilization from organic-bound forms and subsequent Cr-immobilization by means of adsorption and/or crystallization processes with Fe (hydr)oxides, as well as to the transformation of Fe (hydr)oxides after thermal treatments, in accordance with the work of Burton et al. (2019a). The results of sequential extractions (**Figure 3**) show a transformation of Cr species with increasing temperatures from mainly OM-bound fractions to residual fractions, likely being Cr-species strongly bound to Fe (hydr)oxides of increasing crystallinity. Indeed, the extraction procedure adopted for the assessment of the reducible fraction can easily dissolve mainly amorphous iron (hydr)oxides, while crystalline iron (hydr)oxides usually are only barely solubilized, as evidenced by Terzano et al. (2007), especially in the case of Cr. However, we cannot exclude that the increased hydrophobicity of the soils after fire simulations (Arcenegui et al., 2019), could have rendered SEP somewhat ineffective, thus shifting most of the Cr in the last non extractable fraction. Indeed, during fire events soil organic matter (SOM) can undergo structural and compositional modifications, leading to the increase of aromaticity and water repellence of soil (Terzano et al., 2021).

The μXANES mapping performed on A2 soil after heating at 500°C showed the presence of microscopic regions containing Cr(VI) forms within soil aggregates (**Figure 9**). In particular, the LCF performed on Cr μXANES spectra (**Figure 10**) allowed the identification of three Cr-forms: Cr(III)-goethite (46%), chromite (24%), and $CaCrO_4$ (30%). These data confirmed the speciation of Cr obtained by bulk XAS, at least as far as Cr(III) association with Fe (hydr)oxides is concerned, and gave evidence of the partial oxidation of Cr(III) to Cr(VI) after the thermal treatment. In addition, no Cr association with OM was observed in these microscopic areas (about 20-50 μm^2).

All these data suggest that Cr(III) oxidation to Cr(VI) might have occurred only in limited microscopic portions of the sample favored by the presence of Fe-(hydr)oxides, as also reported by Burton et al. (2019a,b) and depletion of OM. It is well known that SOM can readily reduce Cr(VI) (Bartlett, 1997), therefore OM mineralization accelerated by fire events could increase the number of sites where Cr(III) oxidation might occur. As proved by Burton et al. (2019b), fire-induced alterations of iron oxides may favour Cr(VI) formation in soils. Indeed, our results are similar to those observed with larger evidence by Burton et al. (2019b) in a Ferrosol-type soil. These authors suggested that fire-induced heating of Cr(III)-substituted Fe-(hydr)oxides may have the potential to drive Cr(VI) formation and this phenomenon was more evident at temperatures between 400 and

600°C. As stated above, transformations of Fe-(hydr)oxides were faintly observed by high resolution XRPD, with formation of spinel-type minerals at higher temperatures (**Figure S4**).

The soil under investigation had a high content of Ca (9.3% and 11.4% Ca in A1 and A2 soil, respectively; Gattullo et al., 2020). Both µ-XRF analyses (**Figure 5a** and **5b**) and SEM-EDX observations (**Figure 11**) showed the co-presence of Ca, Fe and Cr, especially in the areas of the thin section where Cr(VI) was detected (Figure 9c and 11b). This information can support the observed speciation both for the Cr-Fe(hydr)oxides phases and $CaCrO_4$ formation. No correlation was observed between Cr and Mn. Conversely, Shi et al. (2020) by using XANES, found $CaCrO_4$ in long-term tannery waste contaminated soils, but ascribed the Cr oxidation to Mn-oxides. They proposed a mechanism for Cr(VI) immobilization via precipitation as $CaCrO_4$ and via recrystallization with Fe (hydr)oxides (Shi et al., 2020). Zhou et al. (2021) observed $CaCrO_4$ formation during combustion of tannery sludge residues. Yang et al. (2020), studying the effect of incineration temperature on Cr speciation in Cr-rich tannery sludge, beside observing the formation of $CaCrO_4$ verified that the content of Cr(VI) increases gradually with the increase of temperature from 300°C to 500°C, reaching a maximal level at 500 °C. These authors also proposed that CaO, added for pH adjustment during the physico-chemical treatment process of tannery wastewater in order to ensure the Cr precipitation, was responsible of $CaCrO_4$ formation at high temperatures.

In accordance with all the previously cited findings and literature, we hypothesize that in the investigated soils the Cr(III), once mobilized from complexation with organic molecules after OM burning, was partially oxidized to Cr(VI) within specific microscopic sites containing Fe-(hydr)oxides and CaO, and almost completely deprived of OM. Analysis of µ-XRF maps indeed showed a decrease of the size of soil aggregates (**Figure 5c**) likely due to OM burning. The Cr(VI) was then stabilized via precipitation as $CaCrO_4$. This salt is barely soluble, having a K_{sp} of 7.1×10^{-4} but can be still partially mobilized in aqueous solutions, as proved by the exchangeable Cr(VI) determination (**Figure 4**). Burton et al. (2019b) also observed that 31 - 42% of the total Cr(VI) which formed during heating of the Ferrosol-type soil at 400°C, was exchangeable. This indicates that a substantial portion of Cr(VI) in the heated soil is likely to be readily available and environmentally mobile. It is therefore likely that the Cr(VI) formed during fire-induced soil heating could be readily flushed from fire-impacted surface soil via runoff or rainfall-induced leaching (Burton et al., 2019b). This phenomenon could pose a serious risk to human health if the mobilized Cr(VI) reaches sources of drinking water or is taken up by plants used for human or

animal nutrition. For these reasons, $CaCrO_4$ formation in fire-impacted soils can be considered potentially dangerous for plants and environment, with consequences for human health.

5. Conclusions

The data reported in this study show that apparently stable forms of Cr(III), immobilized and prevented from oxidation to Cr(VI) by large amounts of OM, can become partly mobile and potentially toxic if soils are exposed to high temperatures, as in the case of fires occurrence. This phenomenon can be particularly relevant in agricultural soils amended with compost or biomasses containing high concentrations of Cr since newly formed exchangeable Cr(VI) compounds can be potentially taken up by plants or dispersed in the environment, as well as affect soil (micro)biota. This phenomenon may become more noticeable in the case of high severity fires of higher duration and/or reaching higher temperature than the conditions reported in this study and could also occur in forest soils or wildlands contaminated by Cr, where the mass of burning vegetation is considerably higher. Therefore, this work will provide the basis for further studies aimed at assessing the extent of these processes after wildfires or during in-field simulated fires. Moreover, the presented results offer interesting clues to set up more specific risk assessment studies to appraise the actual consequences of these processes on the environment as well as on plants and soil (micro)organisms.

6. Acknowledgements

We acknowledge DESY (Hamburg, Germany), a member of the Helmholtz Association HGF, for the provision of experimental facilities. Parts of this research were carried out at PETRA III and we would like to thank Jan Garrevoet for assistance in using P06 and Morgane Desmau and Edmund Welter for assistance in using P65. Beamtime was allocated for proposals I-20191116 and EC I-20191119 EC. Moreover, experiments were led also during P06 in-house beamtime. Laboratory X-ray analyses were performed at the Micro X-ray Lab of the University of Bari Aldo Moro (Italy). Ignazio Allegretta was supported by a research grant on the project PON R&I “Studio del sistema suolo-pianta mediante tecniche analitiche innovative che impiegano raggi X” – Progetto

AIM1809249 – attività 1, linea 1. Carlo Porfido was supported by a research grant on PRIN 2017 (Progetti di Ricerca di Rilevante Interesse Nazionale)- 2017BHH84R - "Role of Soil- Plant-Microbial Interactions at Rhizosphere Level on the Biogeochemical Cycle and Fate of Contaminants in Agricultural Soils Under Phytoremediation with Biomass Crops (RIZOBIOREM)."

7. References

Abraham, J., Dowling, K., Florentine, S., 2018. Controlled burn and immediate mobilization of potentially toxic elements in soil, from a legacy mine site in Central Victoria, Australia. Sci. Total Environ. 616–617, 1022–1034. https://doi.org/10.1016/j.scitotenv.2017.10.216

Acosta, J.A., Jansen, B., Kalbitz, K., Faz, A., Martínez-Martínez, S., 2011. Salinity increases mobility of heavy metals in soils. Chemosphere 85, 1318–1324. https://doi.org/10.1016/j.chemosphere.2011.07.046

Adriano, D.C., 2001. Trace Elements in Terrestrial Environments, 2nd ed. Springer-Verlag. https://doi.org/10.1007/978-0-387-21510-5

Alfeld, M., Janssens, K., 2015. Strategies for processing mega-pixel X-ray fluorescence hyperspectral data: A case study on a version of Caravaggio's painting Supper at Emmaus. J. Anal. At. Spectrom. 30, 777–789. https://doi.org/10.1039/c4ja00387j

Allegretta, I., Porfido, C., Martin, M., Barberis, E., Terzano, R., Spagnuolo, M., 2018. Characterization of As-polluted soils by laboratory X-ray-based techniques coupled with sequential extractions and electron microscopy: the case of Crocette gold mine in the Monte Rosa mining district (Italy). Environ. Sci. Pollut. Res. 25, 25080–25090. doi.org/10.1007/s11356-018-2526-9

Arcenegui, V., Jiménez-Morillo, N.T., Jiménez-Pinilla, P., 2019. Soil water repellency, in: Fire Effects on Soil Properties. CRC Press, Taylor & Francis Group, pp. 81–87.

Badía, D., Martí, C., 2003. Effect of simulated fire on organic matter and selected microbiological properties of two contrasting soils. Arid L. Res. Manag. 17, 55–69. https://doi.org/10.1080/15324980301594

Bartlett R.J. (1997). "Chromium redox mechanisms in soils: should we worry about Cr(VI)?", in Chromium Environmental Issues, eds. S. Canali, F. Tittarelli, P. Sequi (Milano, Italy: FrancoAngeli s.r.l.), 1–20

Bartlett, R.J., James, B.R., 1996. Chromium, in: Methods of Soil Analysis, Part 3: Chemical Methods. John Wiley & Sons, Ltd, pp. 683–701.

Brunetti, G., Farrag, K., Soler-Rovira, P., Ferrara, M., Nigro, F., Senesi, N., 2012. Heavy metals accumulation and distribution in durum wheat and barley grown in contaminated soils under Mediterranean field conditions. J. Plant Interact. 7, 160–174. https://doi.org/10.1080/17429145.2011.603438

Burton, E.D., Choppala, G., Vithana, C.L., Karimian, N., Hockmann, K., Johnston, S.G., 2019(a). Chromium(VI) formation via heating of Cr(III)-Fe(III)-(oxy)hydroxides: A pathway for fire-induced soil pollution. Chemosphere 222, 440–444. https://doi.org/10.1016/j.chemosphere.2019.01.172

Burton, E.D., Choppala, G., Karimian, N., Johnston, S.G., 2019(b). A new pathway for hexavalent chromium formation in soil: Fire-induced alteration of iron oxides. Environ. Pollut. 247, 618–625. https://doi.org/10.1016/j.envpol.2019.01.094

Certini, G., 2005. Effects of fire on properties of forest soils: a review. Oecologia 143, 1–10. https://doi.org/10.1007/s00442-004-1788-8

Chandler, C., Cheney, P., thomas, P., Trabaud, L., William, D., 1983. Fire effects on soil, water and air, in: Fire in Forestry. Vol I: Forest Fire Behaviour and Effects. Wiley, New York, pp. 171–202.

Ciavatta, C., Manoli, C., Cavani, L., Franceschi, C., Sequi, P., 2012. Chromium-Containing Organic Fertilizers from Tanned Hides and Skins: A Review on Chemical, Environmental, Agronomical and Legislative Aspects. J. Environ. Prot. (Irvine,. Calif). 03, 1532–1541. https://doi.org/10.4236/jep.2012.311169

Cudennec, Y., Lecerf, A., 2005. Topotactic transformations of goethite and lepidocrocite into hematite and maghemite. Solid State Sci. 7, 520–529. https://doi.org/10.1016/j.solidstatesciences.2005.02.002

del Campillo, M.C., Torrent, J., Loeppert, R.H., 1992. The reactivity of carbonates in selected soils of southern Spain. Geoderma 52, 149–160. https://doi.org/https://doi.org/10.1016/0016-7061(92)90080-Q

Donner, E., Howard, D.L., Jonge, M.D.D., Paterson, D., Cheah, M.H., Naidu, R., Lombi, E., 2011. X-ray absorption and micro X-ray fluorescence spectroscopy investigation of copper and zinc speciation in biosolids. Environ. Sci. Technol. 45, 7249–7257. https://doi.org/10.1021/es201710z

Earnest, C.M., 1991. Thermal analysis of selected illite and smectite clay minerals. Part I. Illite clay specimens, in: Thermal Analysis in the Geosciences. Springer-Verlag, Berlin/Heidelberg, pp. 270–286. https://doi.org/10.1007/BFb0010271

Gattullo, C.E., Allegretta, I., Porfido, C., Rascio, I., Spagnuolo, M., Terzano, R., 2020. Assessing chromium pollution and natural stabilization processes in agricultural soils by bulk and micro X-ray analyses. Environ. Sci. Pollut. Res. 27, 22967–22979. https://doi.org/10.1007/s11356-020-08857-3

Giovannini, C., Lucchesi, S., Giacchetti, M., 1990. Effects of heating on some chemical parameters related to soil fertility and plant growth. Soil Sci. 149, 344–350. https://doi.org/10.1097/00010694-199006000-00005

Grogan, K.L., Gilkes, R.J., Lottermoser, B.G., 2003. Maghemite formation in burnt plant litter at East Trinity, North Queensland, Australia. Clays Clay Miner. 51, 390–396. https://doi.org/10.1346/CCMN.2003.0510404

Guerrero, C., Mataix-Solera, J., Gómez, I., García-Orenes, F., Jordán, M.M., 2005. Microbial recolonization and chemical changes in a soil heated at different temperatures. Int. J. Wildl. Fire 14, 385–400. https://doi.org/10.1071/WF05039

Italian Legislative Decree n. 152 (2006). Decreto legislativo 3 aprile 2006, n. 152. Norme in Materia Ambientale (Gazzetta Ufficiale Della Repubblica Italiana n. 88. Supplemento Ordinario n. 96, 14 aprile 2006)

Johnston, S.G., Karimian, N., Burton, E.D., 2019. Fire promotes arsenic mobilization and rapid arsenic(III) formation in soil via thermal alteration of arsenic-bearing iron oxides. Front. Earth Sci. 7, 139. https://doi.org/10.3389/feart.2019.00139

Kabata-Pendias, A., Mukherjee, A.B., 2007. Trace Elements from Soil to Human. Springer Berlin Heidelberg New York.

Ketterings, Q.M., Bigham, J.M., Laperche, V., 2000. Changes in Soil Mineralogy and Texture Caused by Slash-and-Burn Fires in Sumatra, Indonesia. Soil Sci. Soc. Am. J. 64, 1108–1117. https://doi.org/10.2136/sssaj2000.6431108x

Kumar, V., Chopra, A.K., Kumar, A., 2017. A Review on Sewage Sludge (Biosolids) a Resource for Sustainable Agriculture. Arch. Agric. Environ. Sci. 2, 340–347. https://doi.org/10.26832/24566632.2017.020417

Kumar, P., Kumar, S., Joshi, L., 2015. Socioeconomic and Environmental Implications of Agricultural Residue Burning, SpringerBriefs in Environmental Science. Springer India, New Delhi. https://doi.org/10.1007/978-81-322-2014-5

Lee, S., Kim, Y.J., Moon, H.-S., 1999. Phase Transformation Sequence from Kaolinite to Mullite Investigated by an Energy-Filtering Transmission Electron Microscope. J. Am. Ceram. Soc. 82, 2841–2848. https://doi.org/https://doi.org/10.1111/j.1151-2916.1999.tb02165.x

Li, L., Ishikawa, Y., Mihara, M., 2012. Effects of Burning Crop Residues on Soil Quality in Wenshui, Shanxi of China. Int. J. Environ. Rural Dev. 2012, 30–35.

Lindsay, W.L., Norvell, W.A., 1978. Development of a DTPA Soil Test for Zinc, Iron, Manganese, and Copper. Soil Sci. Soc. Am. J. 42, 421–428. https://doi.org/10.2136/sssaj1978.03615995004200030009x

López-Luna, J., González-Chávez, M.C., Esparza-García, F.J., Rodríguez-Vázquez, R., 2009. Toxicity assessment of soil amended with tannery sludge, trivalent chromium and hexavalent chromium, using wheat, oat and sorghum plants. J. Hazard. Mater. 163, 829–834. https://doi.org/10.1016/j.jhazmat.2008.07.034

Lutz, C., Hampel, S., Beuermann, S., Turek, T., Kunz, U., Garrevoet, J., Falkenberg, G., Fittschen, U., 2021. Determination of the through-plane profile of vanadium species in hydrated Nafion studied with micro X-ray absorption near-edge structure spectroscopy-proof of concept. J. Synchrotron Radiat. 28, 1865–1873. https://doi.org/10.1107/S160057752100905X

Marcos, E., Tárrega, R., Luis, E., 2007. Changes in a Humic Cambisol heated (100-500 °C) under laboratory conditions: The significance of heating time. Geoderma 138, 237–243. https://doi.org/10.1016/j.geoderma.2006.11.017

McGrath, S.P., Zhao, F.J., Lombi, E., 2001. Plant and rhizosphere processes involved in phytoremediation of metal-contaminated soils. Plant Soil 232, 207–214. https://doi.org/10.1023/A:1010358708525

Naidu, R., Biswas, B., Jit, J., Rahman, M.M., 2021. Global assessment of soil pollution: Report. Glob. Assess. soil Pollut. Rep. 8–9. https://doi.org/10.4060/cb4894en

Nordmark, D., Kumpiene, J., Andreas, L., Lagerkvist, A., 2011. Mobility and fractionation of arsenic, chromium and copper in thermally treated soil. Waste Manag. Res. 29, 3–12. https://doi.org/10.1177/0734242X10382819

Panichev, N., Mabasa, W., Ngobeni, P., Mandiwana, K., Panicheva, S., 2008. The oxidation of Cr(III) to Cr(VI) in the environment by atmospheric oxygen during the bush fires. J. Hazard. Mater. 153, 937–941. https://doi.org/10.1016/j.jhazmat.2007.09.044

Pereira, P.; Úbeda, X.; Francos, M. Laboratory fire simulations: Plant litter and soils. In Fire Effects on Soil Properties; CRC Press, Taylor & Francis Group: Leiden, The Netherlands, 2019; pp. 15–38. ISBN 978-1-4863-0815-6

Plante, A.F., Fernández, J.M., Leifeld, J., 2009. Application of thermal analysis techniques in soil science. Geoderma 153, 1–10. https://doi.org/10.1016/j.geoderma.2009.08.016

Rabenhorst, M.C., 1988. Determination of Organic and Carbonate Carbon in Calcareous Soils Using Dry Combustion. Soil Sci. Soc. Am. J. 52, 965–968. https://doi.org/10.2136/sssaj1988.03615995005200040012x

Ravel, B., Newville, M., 2005. ATHENA, ARTEMIS, HEPHAESTUS: Data analysis for X-ray absorption spectroscopy using IFEFFIT. J. Synchrotron Radiat. 12, 537–541. https://doi.org/10.1107/S0909049505012719

Sahuquillo, A., López-Sánchez, J.F., Rubio, R., Rauret, G., Thomas, R.P., Davidson, C.M., Ure, A.M., 1999. Use of a certified reference material for extractable trace metals to assess sources of uncertainty in the BCR three-stage sequential extraction procedure. Anal. Chim. Acta 382, 317–327. https://doi.org/10.1016/S0003-2670(98)00754-5

Sánchez-Monedero, M.A., Mondini, C., De Nobili, M., Leita, L., Roig, A., 2004. Land application of biosolids. Soil response to different stabilization degree of the treated organic matter. Waste Manag. 24, 325–332. https://doi.org/10.1016/j.wasman.2003.08.006

Senesi, N., D'Orazio, V., Ricca, G., 2003. Humic acids in the first generation of EUROSOILS. Geoderma 116, 325–344. https://doi.org/10.1016/S0016-7061(03)00107-1

Shi, J., McGill, W.B., Chen, N., Rutherford, P.M., Whitcombe, T.W., Zhang, W., 2020. Formation and Immobilization of Cr(VI) Species in Long-Term Tannery Waste Contaminated Soils. Environ. Sci. Technol. 54, 7226–7235. https://doi.org/10.1021/acs.est.0c00156

Shukla, K., Kumar, B., Agrawal, R., Priyanka, K., Venkatesh, M., Anshumali, 2017. Assessment of Cr, Ni and Pb Pollution in Rural Agricultural Soils of Tonalite–Trondjhemite Series in Central India. Bull. Environ. Contam. Toxicol. 98, 856–866. https://doi.org/10.1007/s00128-017-2085-7

Silva, M.D.M., Barajas-Aceves, M., Araújo, A.S.F., Araújo, F.F., Melo, W.J., 2014. Soil microbial biomass after three-year consecutive composted tannery sludge amendment. Pedosphere 24, 469–475. https://doi.org/10.1016/S1002-0160(14)60033-3

Solé, V.A., Papillon, E., Cotte, M., Walter, P., Susini, J., 2007. A multiplatform code for the analysis of energy-dispersive X-ray fluorescence spectra. Spectrochim. Acta - Part B At. Spectrosc. 62, 63–68. https://doi.org/10.1016/j.sab.2006.12.002

Sparks, D.L., 1996. Methods of soil analysis, part 3, chemical methods., in: Soil Science Society of America Book Series No 5. Madison, Wis.

Terefe, T., Mariscal-Sancho, I., Peregrina, F., Espejo, R., 2008. Influence of heating on various properties of six Mediterranean soils. A laboratory study. Geoderma 143, 273–280. https://doi.org/10.1016/j.geoderma.2007.11.018

Terzano, R., Rascio, I., Allegretta, I., Porfido, C., Spagnuolo, M., Yaghoubi Khanghahi, M., Crecchio, C., Sakellariadou, F., Gattullo, C.E., 2021 Fire effects on the distribution and bioavailability of potentially toxic elements (PTE) in agricultural soils. Chemosphere 281-130752 https://doi.org/10.1016/j.chemosphere.2021.130752

Terzano, R., Santoro, A., Spagnuolo, M., Vekemans, B., Medici, L., Janssens, K., Göttlicher, J., Denecke, M.A., Mangold, S., Ruggiero, P., 2010. Solving mercury (Hg) speciation in soil samples by synchrotron X-ray microspectroscopic techniques. Environ. Pollut. 158, 2702–2709. https://doi.org/10.1016/j.envpol.2010.04.016

Terzano, R., Al Chami, Z., Vekemans, B., Janssens, K., Miano, T., Ruggiero, P., 2008. Zinc distribution and speciation within rocket plants (Eruca vesicaria L. Cavalieri) grown on a polluted soil amended with compost as determined by XRF microtomography and Micro-XANES. J. Agric. Food Chem. 56, 3222–3231. https://doi.org/10.1021/jf073304e

Terzano, R., Spagnuolo, M., Vekemans, B., De Nolf, W., Janssens, K., Falkenberg, G., Fiore, S., Ruggiero, P., 2007. Assessing the origin and fate of Cr, Ni, Cu, Zn, Pb, and V in industrial polluted soil by combined microspectroscopic techniques and bulk extraction methods. Environ. Sci. Technol. 41, 6762–6769. https://doi.org/10.1021/es070260h

USEPA, 1998. Toxicological review of trivalent chromium (CAS No. 16065-83-1) In Support of Summary Information on the Integrated Risk Information System (IRIS).

USEPA, 1992. Method 7196A. Chromium, hexavalent (colorimetric). United States Environmental Protection Agency, Washington.

USEPA, 1996. Method 3060A. Alkaline digestion for hexavalent chromium. Washington: United States Environmental Protection Agency

Verbinnen, B., Billen, P., Van Coninckxloo, M., Vandecasteele, C., 2013. Heating temperature dependence of Cr(III) oxidation in the presence of alkali and alkaline earth salts and subsequent Cr(VI) leaching behavior. Environ. Sci. Technol. 47, 5858–5863. https://doi.org/10.1021/es4001455

Wolf, R.E., Morman, S.A., Plumlee, G.S., Hageman, P.L., Adams, M.,, 2008. In: Release of Hexavalent Chromium by Ash and Soils in Wildfire-Impacted Areas. USGS Open-File Report, p. 1345.

Yang, Y., Ma, H., Chen, X., Zhu, C., Li, X., 2020. Effect of incineration temperature on chromium speciation in real chromium-rich tannery sludge under air atmosphere. Environ. Res. 183. https://doi.org/10.1016/j.envres.2020.109159

Yu Ling, W., Hui Fang, H., 2006. Effect of Humic Substance on Thermal Treatment of Chromium(VI)-Containing Latosol Soil. J. Air Waste Manag. Assoc. 56, 350–355. https://doi.org/10.1080/10473289.2006.10464464

Welter, E., Chernikov, R. Herrmann, M., Nemausat R. (2019) A beamline for bulk sample x-ray absorption spectroscopy at the high brilliance storage ring PETRA III, AIP Conference Proceedings 2054, 040002 https://doi.org/10.1063/1.5084603

Zavala, L.M., De Celis, R., Jordán, A., 2014. How wildfires affect soil properties. A brief review. Cuad. Investig. Geográfica 40, 311. https://doi.org/10.18172/cig.2522

Zhang, F., Kong, R., Peng, J., 2018. Effects of heating on compositional, structural, and physicochemical properties of loess under laboratory conditions. Appl. Clay Sci. 152, 259–266. https://doi.org/10.1016/j.clay.2017.11.022

Zhou, Y., Chen, Z., Gong, H., Yang, Z., 2021. Chromium speciation in tannery sludge residues after different thermal decomposition processes. J. Clean. Prod. 314. https://doi.org/10.1016/j.jclepro.2021.128071

Figure captions

Figure 1: TGA and DTG curves of a) A1, b) A2 and c) Control soils showing the mass losses that occurred after heating samples from 30°C up to 900°C with a heating rate of 10°C min^{-1}.

Figure 2: (a) Cr-DTPA extractable fraction and (b) Cr in soluble or exchangeable forms (Step 1 of SEP). n.d.: not detectable

Figure 3: Cr fractionation in Control, A1 and A2 soils, before (NT) and after laboratory heating simulations (300°C, 400°C and 500°C); Step 1 (MgCl2): Soluble and exchangeable fraction; Step 2 (CH3COOH): Carbonates bound and acid soluble fraction; Step 3 (NH2OH HCl): Reducible fraction (bound to Fe and/or Mn oxides); Step 4 (H2O2 + HNO3): Oxidisable fraction (bound to OM); Residual fraction: recalcitrant fraction present in the soil at the end of the 4th step.

Figure 4: (a) Total Cr(VI) and (b) exchangeable Cr(VI) concentrations in A1, A2 and control soils before (NT) and after laboratory heating simulation. n.d.: not detectable

Figure 5: a-b, right panels) µ-XRF distribution maps of soil thin sections of the A2 sample treated at 500°C (A2 500 °C) or not-treated (A2 NT). A2 NT and A2 500 °C maps in a) and b) are coloured on the basis of the trends (coloured boxes) identified within the scatterplots shown on the left panel reporting a) the Fe and Cr Kα-lines intensities correlation and b) the Ca and Cr Kα-lines intensities correlation, respectively. c, left panel) Histogram showing the size distribution of soil aggregates containing Cr-Ca-Fe: each dimensional range is colour-coded and used to recolouring the µ-XRF maps (right panels) to visualize particle-size distribution on the thin sections.

Figure 6: Cr XAS spectra of Cr(III) and Cr(VI) reference compounds.

Figure 7: Cr XAS spectra of A2 soils either unheated (A2 NT) and after heating up to 300°C, 400°C and 500°C.

Figure 8: Results of the LCF performed on Cr XAS spectra acquired from A2 bulk soils both before (A2 NT) a) and after laboratory-heating simulations up to 300°C b), 400°C c) and 500°C d).

Figure 9: (a) Micro XRF Cr-distribution map (red pixels) over a thin section of the A2 500°C-heated soil acquired with M4 TORNADO. The yellow rectangle in (a) marks the region within which µXANES mapping was performed. (b) µXANES mapping of part of the yellow-bordered area in (a). (c) Cr-µXANES mapping performed at higher resolution of the area marked with the

cyan rectangle in (b). Red pixels show total Cr distribution while yellow pixels Cr(III)+Cr(VI) distribution. (d) Cr-XANES spectrum of the µXANES map in (b). The ROIs of the total Cr (red) and of the characteristic Cr(VI) pre-edge peak (green) are also reported. (e) Cr-XANES spectrum of the complete map in (c). The white dashed line identified the area from which the spectrum shown in Figure 10 is extracted.

Figure 10: Results of the LCF performed on the Cr µXANES spectrum acquired from the Cr(VI)-containing area (identified by the white dashed line) of Figure 9c.

Figure 11: (a) High definition back scattered detector (HDBSD) image of the area shown in Figure 9c and analysed by µXANES. (b) FEGSEM-EDX elemental distribution of Cr, Ca and Fe. The area surrounded by the white dashed line corresponds approximatively to the yellow area in Figure 9c (slightly rotated). Different colours in (b) correspond to different degrees of overlapping of Cr (red), Ca (green) and Fe (blue).

Graphical abstract

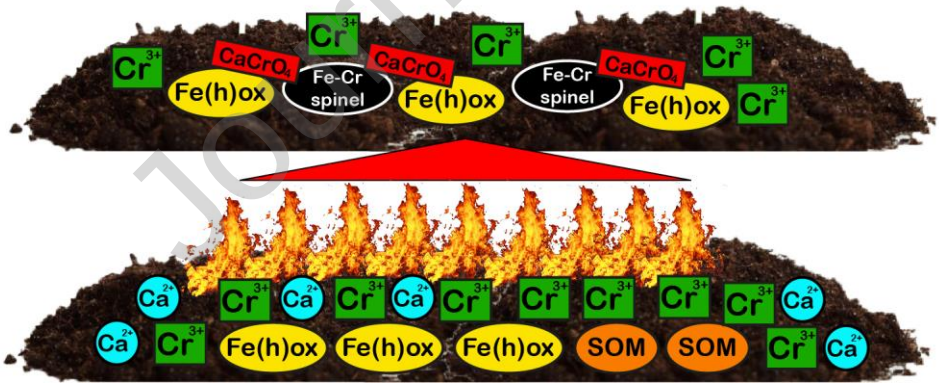

Environmental Implication

In many parts around the globe, tannery waste has been applied to agricultural soils to improve organic matter (OM) content and provide micronutrients for plant nutrition. The high amounts of Cr present in these materials are complexed and stabilized by the OM which also prevents Cr(III) from oxidation to more toxic Cr(VI). However, these materials should be considered hazardous for soils and the environment. Indeed, in this paper we demonstrate that high temperatures, like those that can be reached during a fire on agricultural soils, can change Cr speciation making it potentially more available and more toxic.

Credit Author Statement

Ida Rascio: Methodology, Investigation, Data curation, Writing - Original Draft, Visualization; **Ignazio Allegretta:** Methodology, Software, Formal Analysis, Investigation, Writing - Review & Editing, Visualization; **Concetta Eliana Gattullo:** Methodology, Investigation, Formal Analysis, Writing - Review & Editing; **Carlo Porfido:** Investigation, Software, Formal Analysis, Visualization; **Gian Paolo Suranna:** Methodology, Resources, Writing - Review & Editing; **Roberto Grisorio:** Investigation, Formal Analysis, Writing - Review & Editing; **Kathryn M. Spiers:** Investigation, Methodology, Writing - Review & Editing**; Gerald Falkenberg:** Investigation, Methodology, Writing - Review & Editing, Resources, Supervision; **Roberto Terzano:** Conceptualization, Resources, Writing - Original Draft, Supervision, Funding acquisition.

Declaration of interests

☒The authors declare that they have no known competing financial interests or personal relationships that could have appeared to influence the work reported in this paper.

☐The authors declare the following financial interests/personal relationships which may be considered as potential competing interests:

Highlights

- Agricultural soils amended with tannery waste represent a threat to the environment
- Fires can mineralize soil organic matter (SOM) and modify Cr speciation
- The Cr previously associated to SOM is partly redistributed on iron (hydr)oxides
- A small but significant fraction of Cr(III) is oxidized to $CaCrO_4$
- The newly formed Cr species are potentially accessible for plant uptake